AMERICAN UNIVERSITY OF BEIRUT

EFFECT OF VENTILATION PERIODICITY ON CARBON MONOXIDE FORMATION IN A TRANSIENT FORWARD SMOLDERING CHAR BED

by
ELIE MICHEAL KFOURY

A thesis
submitted in partial fulfillment of the requirements
for the degree of Master of Engineering
to the Department of Mechanical Engineering
of the Faculty of Engineering and Architecture
at the American University of Beirut

Beirut, Lebanon
June 2009

AMERICAN UNIVERSITY OF BEIRUT

EFFECT OF VENTILATION PERIODICITY ON CARBON MONOXIDE FORMATION IN A TRANSIENT FORWARD SMOLDERING CHAR BED

by

ELIE MICHEAL KFOURY

Approved by:

Dr. Alan Shihadeh, Associate Professor Mechanical Engineering	Advisor
Dr. Issam Lakkis, Assistant Professor Mechanical Engineering	Co-advisor
Dr. Nesreen Ghaddar, Professor Mechanical Engineering	Member of Committee

Date of thesis defense: June 2, 2009

AMERICAN UNIVERSITY OF BEIRUT

THESIS RELEASE FORM

I, Elie Micheal Kfoury

☐ authorize the American University of Beirut to supply copies of my thesis to libraries or individuals upon request.

☐ do not authorize the American University of Beirut to supply copies of my thesis to libraries or individuals for a period of two years starting with the date of the thesis defense.

_____

Signature

_____

Date

ACKNOWLEDGMENTS

Special thanks to my advisors Dr. Alan Louis Shihadeh and Dr. Issam Lakkis for their guidance, support, and patience. My thanks goes also to Dr. Nesreen Ghaddar for her support, encouragement, and trust. You have all been the best of advisors one may ask for.

AN ABSTRACT OF THE THESIS OF

Elie Micheal Kfoury for Master of Engineering
Major: Mechanical Engineering

Title: Effect of Ventilation Periodicity on Carbon Monoxide Formation in a Transient Forward Smoldering Char Bed

Laboratory measurements of smoked tobacco products are routinely performed to compare toxicant and carcinogen yields across products and to provide information on potential health hazards arising from the use of these products. Standard cigarette smoke measurement methods have for the past 50 years utilized a steady periodic puffing regimen (i.e. a fixed puff volume, puff duration, and interpuff interval) to produce the test smoke for toxicant yield analyses. While using a steady periodic regimen simplifies the test procedure, smoothing the highly variable puffing characteristic of real smoking may bias the production of combustion-generated toxicants because combustion kinetics is highly non-linear. This thesis aims to study the effect of representing real puffing behavior with a steady periodic puffing model by comparing experimental carbon monoxide yields generated with a machine programmed to use real and steady periodic puffing regimens.

To do so, smoking topography recordings from 38 human subjects in Beirut area cafés were reproduced ("played-back") using a digital smoking machine and the resulting CO yields measured. Steady periodic representations of these 38 smoking topography recordings were then also run through the smoking machine, and the CO yields were again measured and compared to those measured with the playback sessions. It was found that real smoking sessions produce 16% more CO than their equivalent steady periodic sessions. These experiments also showed that the CO yield is negatively correlated with flow rate (a greater flow rate causes a decrease in CO yield).

To understand the phenomena underlying the relationship between ventilation periodicity and smoke toxicant yields, a one-dimensional transient forward smoldering charcoal bed model (which represents the burning charcoal on a narghile head) was developed and implemented numerically. Using simplified 3-step chemistry, the model simulates the smoking process and calculates the CO yield for any input ventilation regimen. The computational model agreed with the experiments in showing that real smoking sessions produce more CO than their steady periodic equivalents (23% on average). Parametric variation showed that flow rate variability, and not variability in puff duration or interpuff interval, causes a real smoking session to exhibit higher CO yields than its steady periodic analog. Simulations indicate that this effect is derivative of slow chemistry relative to thermal convection in the ventilation regime of this problem.

CONTENTS

ILLUSTRATIONS

Figure Page

TABLES

CHAPTER 1

INTRODUCTION

Narghile waterpipe smoking has been practiced extensively for more than four hundred years [21]. This smoking practice is spreading widely recently [18]. A noticeable increase in the use of the waterpipe smoking has been noted in recent years in south-west Asia and North Africa, particularly among young people [19, 20]. Several studies have shown the health risks involved in inhaling the smoke of a narghile [22-25]. Among the toxic matter found in narghile products, carbon monoxide is present in large quantities. A comparison between wood and charcoal fired stoves shows that CO and CO_2 emission factor values for wood (1560-1620g/Kg for CO_2, 19-136 g/Kg for CO) are lower compared to charcoal (2155-2567g/Kg for CO_2, 35-198 g/Kg for CO) [26], which demonstrates the significant amounts of CO produced by charcoal combustion.

The toxicity of carbon monoxide has been summarized by Monzer et al. [16]. The following description is a summary of the findings of this author.

> "CO is a ubiquitous asphyxiant, colorless, non-irritant, odorless gas that acts as a cellular poison. Exposure to carbon monoxide especially affects unborn babies, infants, and people with anemia or a history of heart or respiratory disease. Breathing low levels of CO can cause fatigue and increase chest pain in people with chronic heart disease. Breathing higher levels of carbon monoxide causes flu-like symptoms such as headaches, dizziness, and weakness in healthy people. Carbon monoxide also causes sleepiness, nausea, vomiting, confusion, and disorientation. At very high levels, it causes loss of consciousness and death. Several fatalities occur every year from carbon monoxide exposure related to residential combustion appliances, and thousands of people become ill or seek medical attention [15, 32, and 33]. It displaces oxygen from oxyhaemaglobin causing tissue asphyxia, and also acts as cellular poison. Tissues with a high metabolic rate, such as the heart and the brain, will incorporate CO faster. CO acts as an exogenous and cell poison as well, thus having two intense modes of toxicity [13, 27, 28]. Even low concentrations of CO for a prolonged period caused leucoencephalopathy in un-anaesthetized sheep

> [15]. Long-term exposure to low levels of CO as with smokers has been identified as one of the most important contributors to smoking-related diseases especially coronary heart diseases [29]".

Carbon Monoxide (CO) is a toxic gaseous species that results from the incomplete oxidation of carbon in a limited oxygen supply. The health effects of carbon monoxide call for accurate methods to study its production in widespread smoking devices. Standard methods of cigarette experimentation using a smoking machine call for a given number of uniformly spaced puffs of fixed duration and volume. In other words, the real stochastic puffing patterns observed for smokers are replaced by an equivalent periodic and homogeneous puffing pattern. The effect of such a smoking model on CO production has never been studied, and this may be particularly important for narghile smoking which is characterized by hundreds of irregularly spaced puffs of varying volumes. The comparison between the real (stochastic) puffing pattern and its equivalent periodic pattern has never been done before for a narghile waterpipe. It is the subject of this thesis to assess the effect of puffing-resting topography on the production of CO. We would like to know to the impact of representing a real smoking session with its periodic analog to quantify the amount of CO produced.

This thesis thus aims to study the phenomenon of carbon monoxide production in the burning charcoal of a narghile waterpipe. The main goal of this work is to compare the carbon monoxide yield from a stochastic (real) smoking session and an equivalent periodic-smoking-pattern session. The end goal of this study would be to determine whether a real (random puffing) smoking pattern could be properly represented by its equivalent periodic scheme in terms of carbon monoxide (and other particulate matter) production in smoking

machine studies of toxicant yield. In order to answer the latter question, several real-life smoking sessions (data collected from Beirut Cafes, Shihadeh et al. [2]) will be experimentally reproduced ("played back") and then the CO yield of these real sessions will be compared to the yield from their equivalent steady periodic sessions. On the other hand, a numerical simulation code will be employed to simulate the same experimental smoking sessions in order to shed light on the physical phenomena underlying the experimental observed trends of CO yields.

Most of the carbon monoxide produced in the smoking products of a narghile waterpipe originates in the burning charcoal (which is used as a heat source that ensures the continuation of the smoldering process in the tobacco) [16, 17].Thus, in order to evaluate the amount of carbon monoxide produced in a narghile, it is sufficient to evaluate the quantity of CO produced in the charcoal of that narghile. Therefore, a basic model (based on fundamental physics) that represents fixed bed charcoal combustion will be developed. The model will be simplified to keep the computational effort as small as possible without sacrificing the inclusion of the most essential phenomena that govern the combustion process. The conservation laws (mass and energy) will be applied to the charcoal. The solution of these conservation laws will provide temperature and species concentrations within the charcoal.

The above mentioned partial differential equations will be solved numerically. This solution will allow for the transient analysis of the behavior of the charcoal system. It is sought to understand what physical parameters interact to produce the specific patterns of system behavior subject to a random versus periodic forcing function.

CHAPTER 2

LITERATURE REVIEW

Fixed bed combustion of solid fuels is the most common combustion process in industrial applications of charcoal combustion such as biomass conversion, waste incineration, and small scale distinct energy systems [15, 49, and 50]. Packed bed combustion is the most widespread form of utilizing charcoal fuels (cooking, heating, water-pipe smoking, and so on). The phenomenon of fixed bed combustion involves various complicated processes of multi-physical disciplines. These processes may be summarized as follows:

- Homogeneous chemical reactions: those are the chemical transformations that involve gaseous species as reactants.
- Heterogeneous chemical reactions: those are solid-gas chemical interactions. Heterogeneous reactions involve mass transfer between the solid and gaseous phases.
- Solid phase heat transfer: these processes include radiative, the conductive heat transfer mechanisms among solid (fuel) particles, and the heat of chemical reactions that occur within the solid.
- Gas phase heat transfer: this process involves conduction among the gaseous particles and the heat of chemical reactions (occurring in the gas phase).
- Solid-gas heat transfer: these are the radiative and convective heat transfer processes occurring between the solid and gaseous phases.

- Physical changes of solid particles: those changes gradually arise as combustion proceeds. These transformations include: particle expansion/shrinking, fragmentation, internal pore formation, sintering, elutriation, and melting [49].

- Ash formation: this is due to the incombustible mineral content of charcoal. Formation of the ash layer has drastic effects on the transfer and chemical phenomena that occur in a burning bed.

The above processes may be modeled by using the following laws applied for fixed bed combustion:

- Solid mass continuity.

- Solid components continuity.

- Solid energy conservation: including sensible energy loss from the solid phase, chemical energy source from reactions occurring within the solid phase, conductive heat transfer within the solid phase, convective heat transfer between solid and gas phases, radiative heat transfer among solid particles.

- Gas mass continuity.

- Gas species continuity.

- Gas energy conservation: including processes that are analogous to the solid energy balance.

- Pressure variations: captured with the momentum equation for the gaseous flow within the packed bed.

- Modeling physical changes: shrinkage, fragmentation, and generation of internal pores.

- Ash modeling: including the effect of ash on the transport equations and heat transfer phenomena.
- Chemical reactions: including oxidation of the fuel (charcoal in this case).

Each of the previously mentioned laws have been studied and modeled by several authors. It is the intent of this review to summarize the work done on each of these topics. The literature review presented here is for modeling transient fixed bed combustion of solid fuels in one spatial dimension. Extension to multi dimensional models is possible, but is out of the scope of this paper.

A. Solid Mass Continuity

Solid mass continuity translates into a mass balance performed on a control volume that contains the solid phase. The general form of the solid mass conservation equation in a fixed bed is given per unit volume of bed as [49]:

$$\frac{\partial \rho_s (1-\varepsilon)}{\partial t} + \frac{\partial \rho_s v_s}{\partial y} = -\dot{\mathrm{M}}_{s\to g}$$

Where ρ_s is the density of the solid phase, ε is the bed porosity, v_s is the superficial (Darcean) velocity of the solid particles, $\dot{\mathrm{M}}_{s\to g}$ is the mass rate of change of solid fuel to gaseous products (gasification).

This solid mass conservation law is needed for modeling physical changes that occur during the combustion in fixed beds.

Bhagat [51] examined wood charcoal combustion and the effect of the ash layer on the kinetics of oxidation. He concluded that $\dot{\mathrm{M}}_{s\to g}$ is given as $\dot{\mathrm{M}}''_{s\to g} = 475 P_{O_2} e^{\left(\frac{-12000}{T_s}\right)}$.

Hayhurst [50] studied mass transfer processes for carbon particles reacting with oxygen and concluded that the rate of carbon oxidation per particle is given as:

$$Q = \pi d.Sh_{EMCD}.\frac{PD_1}{RT_m}.(X_b - X_s) + 2\pi d.Sh_{EMCD}.\frac{PD_1}{RT_m}.\ln\left(\frac{1+X_b}{1+X_s}\right) + \pi d.Sh_{EMCD}.\frac{P}{R}.\left\{\frac{D_1 X_b}{T_b} + \frac{D_2}{T_s}\ln\left(\frac{1+X_b}{1+X_s}\right)\right\}$$

Where d is the solid particle diameter. $Sh_{EMCD} = 2 + 0.69\,\mathrm{Re}^{1/2}\,Sc^{1/3}$ is the equimolar counter diffusion Sherwood number. P is the total pressure. D_1 is the diffusion coefficient of oxygen into carbon. D_2 is the diffusion coefficient of carbon dioxide into carbon. R is the universal gas constant. T_m is the mean temperature of the solid and gaseous phases. X_b is the mole fraction of oxygen in the bulk gas. X_s is the mole fraction of oxygen at the solid phase surface. T_b is the gas temperature in a region far from the solid particle. T_s is the temperature in the gas near the solid particle.

In general, the solid mass conservation equation is solved for $\rho_s v_s$. This result is then used in the equations that model physical changes in fixed bed combustion. Such phenomena will be discussed in later sections.

B. Solid Components Continuity

The solid mass component continuity is a mass balance of solid species performed on a control volume that contains the solid phase. The general form of the solid species conservation equation in a fixed bed is given per unit volume of bed as [49, 52]:

$$\frac{\partial \rho_s (1-\varepsilon) Y_{s,i}}{\partial t} + \frac{\partial}{\partial y}\left(\rho v_s Y_{s,i}\right) - \sum_{i,s}\frac{\partial}{\partial y}\left(\rho_s Y_{s,i} D_{eff,i,s}\Lambda^{-2}\frac{\partial Y_{s,i}}{\partial y}\right) = \dot{\mathrm{M}}_{s,i}$$

Where ρ_s is the density of the solid phase, ε is the bed porosity, v_s is the Darcean (superficial) velocity of the solid particles, $Y_{s,i}$ is the mass fraction of the i[th] component of the solid phase, $\sum_{i,s}$ is a summation over the solid species, $D_{eff,i,s}$ is the effective molecular diffusion coefficient of the solid component i into the solid phase, Λ is the volume fraction that relates the volume of the solid phase to its initial volume as $\Lambda = V/V_{initial}$, $\dot{M}_{s,i}$ is the mass rate of change of species i of the solid material.

This solid component conservation law is needed for modeling ash formation and transport. Ash modeling will be discussed in a later section.

C. Solid Energy Conservation

The solid energy equation per unit bed volume is given as [49, 52, 55]:

$$\frac{\partial \rho_s (1-\varepsilon) h_s}{\partial t} + \frac{\partial \rho_s v_s h_s}{\partial y} - \sum_{i,s} \frac{\partial}{\partial y}\left(h_s \rho_s Y_{s,i} D_{eff,i,s} \Lambda^{-2} \frac{\partial Y_{s,i}}{\partial y} \right) = q_{chem,s} - q_{thermal,s\to g} + q_{cond,s} + q_{conv,s-g} + q_{rad,s}$$

Where ρ_s is the density of the solid phase, ε is the bed porosity, h_s is the specific enthalpy of the solid phase, v_s is the superficial (Darcean) velocity of the solid particles, $\sum_{i,s}$ is a summation over the solid species, $Y_{s,i}$ is the mass fraction of the i[th] component of the solid phase, $D_{eff,i,s}$ is the effective molecular diffusion coefficient of the solid component i into the solid phase, Λ is the volume fraction that relates the volume of the solid phase to its initial volume, $q_{cond,s}$ is the conductive heat transfer within the solid phase, $q_{conv,s-g}$ is the convective heat transfer between the solid and the gaseous phases, $q_{rad,s}$ is the radiative

heat transfer within the solid phase, $q_{chem,s}$ is the chemical heat released in the solid phase, $q_{thermal,s\to g}$ is the thermal heat carried out of the solid phase by solid to gas mass transfer.

The terms appearing in the right hand side of the solid energy equation represent the heat transfer mechanisms within the solid phase inside the bed. Below is a discussion of each of these terms.

1. Sensible Energy Loss from the Solid Phase

The thermal enthalpy lost from the solid phase represents the sensible energy loss from the mass transfer from the solid to the gaseous phase (gasification). When modeling this heat transfer phenomena in fixed beds, two levels of spatial discretization evolve. The first one uses a simple one dimensional scheme that treats fuel material as stacked layers. The other school employs a two dimensional Cartesian grid and treats the solid fuel as a segregation of discrete particles.

a. <u>One Dimensional Scheme</u>

When fuel material (charcoal here) is modeled as stacked layers, the sensible energy loss from the solid phase may be expressed as [49, 52, 55]:

$$q_{thermal,s\to g} = \dot{\mathrm{M}}_{s\to g} h_s = \dot{\mathrm{M}}_{s\to g} C_{P,s} \mathrm{T}_s$$

Where $\dot{\mathrm{M}}_{s\to g}$ is the mass rate of change of solid fuel to gaseous products (gasification), $C_{P,s}$ is the specific heat of the solid phase, T_s is the solid phase temperature.

b. Discrete Particle Method

Some authors use discrete particle methods to account for the thermal energy transfer within the solid phase. This school of fixed bed modeling uses finite volume techniques to solve the conservation equations on a Cartesian grid. For example, Burch et al. [53] suggest using a model that consists of n discrete solid particles whose total thermal energy is the summation of individual particles. This summation is carried out over all the solid species. Thus,

$$q_{thermal,s\to g} = \sum_{k=1}^{n}\sum_{j=1}^{m} \frac{1}{\Delta t}\int \left(C_{p,Solid}\dot{m}_{Solid,j,k}\mathrm{T}_{Solid,k}\right)dt$$

Where $\sum_{k=1}^{n}$ is the summation over the discrete solid particles, $\sum_{j=1}^{m}$ is the summation over all the gas species, $C_{P,Solid}$ is the specific heat of the solid phase, $\mathrm{T}_{Solid,k}$ is the temperature of the solid particle 'k', $\dot{m}_{Solid}$ is the mass loss rate of solid species j.

The value of the specific heat of the fuel (charcoal in this case), is a subject of big disagreement among many workers. This parameter is sensitive to many factors as the type and structure of the original wood, the pyrolysis and carbonization conditions, and the structure of the obtained charcoal, rendering it impossible to report typical values. In general, two schools emerge: one that supports using constant values for the specific heat, while the other advocates temperature dependant forms. For example, Larfeldt et al. [25] present a review of heat transport properties of charcoal obtained from large wood particles. They found that the temperature dependent specific heat is reported as:

$$C_{p,charcoal}(\mathrm{T}) = 1430 + 0.355\mathrm{T} - \frac{732*10^5}{\mathrm{T}^2}$$

In another study, Gupta et al. [57] recommend using C_p for softwood chars as:

$$C_{p,charcoal}(\mathrm{T}) = -0.0038\mathrm{T}^2 + 5.98\mathrm{T} - 795.28$$

On the other hand, Gronli [61] studied the degradation of biomass and reviewed reported values for constant specific heat for charcoal. He found that these reported values (at room temperature) range from 670 to 1350 J/Kg. °K.

Larfeldt et al. made a comparison between using constant versus temperature dependant specific heat values. The comparison was performed between the constant values reported by Gronli and their temperature dependent function (given above). They recommended that it is best to use a constant average value of 1000 J/Kg. °K. The reason behind this is that the temperature dependences of the thermal conductivity and that of the specific heat cancel each other.

2. Chemical Energy Source from Reactions Occurring within the Solid Phase

This class represents the energy release/absorption from heterogeneous solid-gas chemical reactions.

$$q_{chem} = \dot{\mathrm{M}}_{s\to g}\Delta\mathrm{H}_r$$

Where $\dot{\mathrm{M}}_{s\to g}$ is the mass rate of change of solid fuel to gaseous products (gasification), ΔH_r is the heat of reaction for heterogeneous solid-gas chemical reactions.

3. Conductive Heat Transfer within the Solid Phase

The heat conducted among the particles of the solid phase is given in several forms. Yang et al. [49], Cooper et al. [55], and Leach et al. [54] propose using Fourier's law of conduction; then,

$$q_{cond,s} = \frac{\partial}{\partial y}\left[(1-\varepsilon)k_s \frac{\partial \mathrm{T}_s}{\partial y}\right]$$

Where ε is the porosity fraction of the bed, k_s is the thermal conductivity of the solid phase, T_s is the temperature of the solid phase.

Thunman et al. [52] also use Fourier's law to account for conductive heat transfer within the solid phase; but they propose using the volume fraction, Λ, instead of the void fraction. This accounts for physical changes that occur in the solid structure; then,

$$q_{cond,s} = \frac{\partial}{\partial y}\left[\Lambda^{-2} k_s \frac{\partial \mathrm{T}_s}{\partial y}\right]$$

The value of the thermal conductivity in highly porous chars (such as charcoal) continues to be one of the most studied issues in heat transfer phenomena of solid fuels. Many experimental methods have been developed for this purpose. For example, Kantorovich and Bar-Ziv [26] suggest using experimental methods that employ measurements of the photophoretic force F_{ppf} to calculate the char thermal conductivity by the relation

$$F_{ppf} = \frac{-3\pi\mu^2 d_{eff}(\varepsilon_e \mathrm{I})}{4(k_p + k_g)\mathrm{T}\rho_g} = mg\,\frac{36\mu^2}{g\rho_g\rho(d^o)^3\gamma}\cdot\frac{\mathrm{T}-\mathrm{T}_g}{\mathrm{T}}\cdot\frac{k_g}{k_p - k_g}$$

Where μ is dynamic viscosity of the gas phase, d_{eff} is the effective char particle diameter, ε_e is the emissivity, I is the intensity of laser in the experiment, k_p is the thermal conductivity of the char, k_g is the gaseous phase thermal conductivity, T is the particle temperature, ρ_g is the gas phase density, ρ is the particle density, T_g is the char particle periphery temperature.

Other authors prefer to use constant thermal conductivities. As an example Larfeldt et al. [25] performed a comparative study between using constant and temperature dependant values. They recommended the use of constant char thermal conductivity. On the other hand, many workers prefer using temperature dependent values. For example, Gupta et al. [57] performed experiments on the thermal properties of softwood char. They report a particle thermal conductivity of 0.0946 W/m.°K at 300°K that follows a linear relation with temperature.

Other authors like Burch et al. [53] for example, model heat conduction using a discrete particle method. In such methods, finite heat differences on a Cartesian grid are evaluated. The most distinctive feature of these models is that it presents a "contact area" between neighboring particles (similar to that of gearing mechanisms) to calculate the effective conductive area of discrete particles. Thus for a contact angle of γ the effective area is:

$$\mathrm{A}_c = \frac{1}{2}\left(\left(R_1 \tan\gamma\right)^2 + \left(R_2 \tan\gamma\right)^2\right)$$

Where R_1 and R_2 are the radii of contact particles.

4. Convective Heat Transfer between Solid and Gas Phases

In charcoal combustion, convective heat transfer occurs due to the movement of gas within the porous structure of the char [26]. For this heat transfer mode to be effective, two conditions need to be satisfied. The first is that intensive circulation of the gas within the pores needs to be established (Pe>1000). The second stipulation is that the average pore sizing must be more than one centimeter [26].

In general, convective heat transfer within burning charcoal is simple in form, and may be written as [49, 52, 54, 55]:

$$q_{conv,s-g} = h_{conv} \mathrm{A}_s \left(\mathrm{T}_g - \mathrm{T}_s \right)$$

The convective heat transfer coefficient h_{s-g} is determined using the relations of the Nusselt number, $Nu = \dfrac{h_{s-g} * d_{char\ particle}}{k_{gas}}$. Several authors give different relations for the Nusselt number. Wakao et al. [58] suggest that for packed beds:

$$Nu = 2 + 1.1 \mathrm{Re}^{0.6}\, \mathrm{Pr}^{1/3} = 2 + 1.1 \left(\frac{\varepsilon . V_g . d_{particle}}{\upsilon} \right)^{0.6} \left(\frac{\upsilon}{\alpha} \right)^{1/3}$$

Where Re is the Reynolds number calculated with respect to the diameter of the solid particle, Pr is the Prandtl number for the gaseous phase, ε is the bed porosity, V_g is the gas flow velocity, $d_{particle}$ is the diameter of a solid particle, υ is the kinematic viscosity of the gas phase, α is the thermal diffusivity of the gas phase.

Bhagat [51], experimentally determined that:

$$Nu = 2.6(\mathrm{Re}.\mathrm{Pr})^{0.38} = 2.6\left(\frac{\varepsilon.V_g.d_{particle}}{\alpha}\right)^{0.38}$$

As in the case of thermal energy transfer, some workers model the convective heat transfer in fixed beds using a discrete model. This involves evaluating the convection heat transfer at discrete particles and then summing over the whole grid. Bruch et al. [53] proposes using time-averaged temperature differences to evaluate this summation:

$$q_{conv,s-g} = \sum_{k=1}^{n} h_k A_k \frac{1}{\Delta t}\int_0^{\Delta t}\left(\mathrm{T}_{g,k} - \mathrm{T}_{g,i}\right)dt$$

Where $\sum_{k=1}^{n}$ is the summation over the discrete solid particles, h_k is the convective heat transfer coefficient calculated for the kth particle, A_k is the surface area of the kth solid particle, $\mathrm{T}_{g,k}$ is the temperature of the gas near the kth particle, $\mathrm{T}_{g,i}$ is the gas temperature in cell i. Δt is the time lapse.

5. Radiative Heat Transfer among Solid Particles

In fixed bed combustion, radiative heat transfer occurs due to absorption-emission or scattering of radiation by the pore walls [26]. The contribution of radiative heat transfer increases with temperature. For temperatures that are lower than 1000°K, radiation effects can be neglected (especially if the solid is a weak conductor like chars) [26]. On the other hand, radiation heat transfer is heavily dependant on the diametrical size of the pores. In fact, only pore sizes that are above 50μm contribute to the radiation heat transfer phenomenon [25]. Therefore, several authors often neglect radiation interactions within packed beds (for example Leach et al. [54], Cui et al. [60], and Cooper et al. [55]). Other

authors recommend modeling radiative heat transfer. They propose several methods for quantifying radiations in packed beds. Yang et al. [49] and Thunman et al. [52] propose the two flux method used with the Schuster-Schwartzschild approximation. This gives:

$$q_{rad} = \pi \frac{\partial}{\partial y}\left(J^{+} + J^{-}\right)$$

Where J^{+} is the positive radiative intensity, J^{-} is the negative radiative intensity. These two values are obtained by solving the following system of differential equations:

$$\frac{1}{2}\frac{\partial J^{+}}{\partial \kappa} = \varepsilon_{rad}\frac{\sigma T^{4}}{\pi} - J^{+} + \frac{1-\varepsilon_{rad}}{2}\left(J^{+} + J^{-}\right)$$

$$\frac{1}{2}\frac{\partial J^{-}}{\partial \kappa} = \varepsilon_{rad}\frac{\sigma T^{4}}{\pi} + J^{-} - \frac{1-\varepsilon_{rad}}{2}\left(J^{+} + J^{-}\right)$$

Where κ is the optical depth defined as $\kappa = \int_{0}^{y} \frac{\Lambda\left(A_{eff}\right)}{4} dy$, ε_{rad} is the emissivity, σ is the Stefan-Boltzmann constant.

Another group of radiation modelers (Larfeldt et al. [25] and Kantorovich et al. [26]), propose including radiation into the effective thermal conductivity. This effective thermal conductivity will thus include effects of solid and gas conduction as well as radiation within the solid phase:

$$k_{eff} = (1-\varepsilon)k_{solid} + \varepsilon k_{gas} + k_{rad}$$

Two expressions are given for k_{rad}. The first expression is [26]:

$$k_{rad} = 4\sigma\varepsilon_{e} n^{2} R T^{3}$$

Where: σ is the Stefan-Boltzmann constant, ε_{e} is the pore surface emissivity, n is the index of refraction of the gas. R is the radius of the pore. T is the absolute temperature.

Another expression for the radiative thermal conductivity is given by [25]:

$$k_{rad} = 4.\sigma.\varepsilon_g^{macro}.\psi.d_{pore}^{macro}.T^3$$

Where: σ is the Stefan-Boltzmann constant, ε_g^{macro} fractional volume occupied by large pores. ψ is the pore surface emissivity, d_{pore}^{macro} is the diameter of the large pores. T is the absolute temperature.

D. Gas Mass Continuity

The gas mass conservation law is given per unit bed volume as [49, 52, 55]:

$$\frac{\partial \rho_g \varepsilon}{\partial t} + \frac{\partial \rho_g v_g}{\partial y} = \dot{\mathrm{M}}_{s \to g}$$

Where ρ_g is the density of the gaseous phase, ε is the bed porosity, v_g is the velocity of the gaseous flow through the bed, $\dot{\mathrm{M}}_{s \to g}$ is the mass rate of change of solid fuel to gaseous products (gasification).

E. Gas Species Continuity

The gas species mass conservation law is given per unit bed volume as [49, 52, 55]:

Yang, Ryu, Choi: $\frac{\partial \varepsilon \rho_g Y_{i,g}}{\partial t} + \frac{\partial \rho_g v_g Y_{i,g}}{\partial y} - \sum_{i,g} \frac{\partial}{\partial y}\left(\rho_g D_{eff,i,g} \Lambda^{-2} \frac{\partial Y_i}{\partial y} \right) = \dot{\mathrm{M}}_{g.i}$

Where ε is the bed porosity, ρ_g is the density of the gaseous phase, $Y_{i,g}$ is the mass fraction of the ith component of the gaseous phase, $\sum_{i,g}$ is a summation over the gaseous

species, $D_{eff,i,g}$ the effective molecular diffusion coefficient of the gaseous component i into the solid phase, v_g is the velocity of the gaseous flow through the bed, $\dot{M}_{g,i}$ is the mass rate of the change of the i[th] gaseous species.

F. Gas Energy Conservation

The gas energy equation is given per unit bed volume as [49, 52, 55]:

$$\frac{\partial}{\partial t}\left(\varepsilon\rho_g h_g\right)+\frac{\partial}{\partial y}\left(\rho_g v_g h_g\right)-\sum_{i,s}\frac{\partial}{\partial y}\left(h_g\rho_g Y_{g,i} D_{eff,i,g}\Lambda^{-2}\frac{\partial Y_{g,i}}{\partial y}\right)=q_{cond,g}+q_{conv,s-g}+q_{rad,g}+q_{chem,g}+q_{thermal,s\to g}$$

Where ε is the bed porosity, ρ_g is the density of the gas phase, h_g is the specific enthalpy of the solid phase, v_g is the velocity of the gaseous flow through the bed, $Y_{g,i}$ is the mass fraction of the i[th] component of the gas phase, $\sum_{i,g}$ is a summation over the gaseous species, $D_{eff,i,g}$ is the effective molecular diffusion coefficient of the gas component i into the gas phase, Λ is the volume fraction that relates the volume of the solid phase to its initial volume, $q_{cond,g}$ is the conductive heat transfer within the gas phase, $q_{conv,s-g}$ is the convective heat transfer between the solid and the gaseous phases, $q_{rad,g}$ is the radiative heat transfer within the gas phase, $q_{chem,g}$ is the chemical heat released in the gas phase, $q_{thermal,g}$ is the thermal heat gain carried in to the gas phase by solid to gas mass transfer. The expressions given for heat transfer mechanisms in the gas phase are analogous to those of the solid phase explained earlier. Radiation heat transfer within the gas phase is often neglected. Thus,

$$q_{cond,g} = \frac{\partial}{\partial y}\left(k_{eff,g} \frac{\partial \mathrm{T}_g}{\partial y} \right)$$

$$q_{conv,s-g} = h_{s-g} a_B \left(\mathrm{T}_s - \mathrm{T}_g \right)$$

$$q_{rad,g} = 0$$

$$q_{chem} = \dot{\mathrm{M}}_{s \to g} \Delta \mathrm{H}_r$$

$$q_{thermal,s \to g} = \dot{\mathrm{M}}_{s \to g} C_{p,s-g} \mathrm{T}_s$$

G. Pressure Variations

Pressure variations within a burning fixed bed are often neglected. However, some fixed bed combustion modelers choose to couple the pressure and the velocity fields. This requires introducing a momentum equation into the basic model. In such models, the pressure variable appears in both the momentum and the energy equations [53].

Burch et al. [53] studied wood combustion in fixed beds; they use a momentum equation in the form of:

$$\frac{\partial}{\partial t}\left(\rho_g v_g\right) + \nabla\left(\rho_g v_g^2\right) = -\nabla p - \frac{\mu}{K} v_g$$

Where ρ_g is the density of the gas phase, v_g is the velocity of the gaseous flow through the bed, ∇p represents pressure variations within the bed, μ is the dynamic viscosity, K is the permeability.

When accounting for the pressure drop in the bed, the pressure term appears in the gas energy equation. Thus,

$$\frac{\partial}{\partial t}\left(\rho_g C_{p,g} \mathrm{T}\right) + \nabla\left(\rho_g v_g C_{p,g} \mathrm{T}\right) = -\nabla p v_g + q_{con,g} + q_{chem,g} + q_{thermal,g} + q_{conv,s-g} + q_{rad,g}$$

Where ρ_g is the density of the gas phase, $C_{p,g}$ is the specific heat of the gas phase, T is the temperature, v_g is the velocity of the gaseous flow through the bed, ∇p represents pressure variations within the bed, $q_{cond,g}$ is the conductive heat transfer within the gas phase, $q_{conv,s-g}$ is the convective heat transfer between the solid and the gaseous phases, $q_{rad,g}$ is the radiative heat transfer within the gas phase, $q_{chem,g}$ is the chemical heat released in the gas phase, $q_{thermal,g}$ is the thermal heat gain carried in to the gas phase by solid to gas mass transfer.

H. Modeling Physical Changes

As solid fuels burn in fixed beds, the internal micro structure of the fuel undergoes various transformations. These may be summarized by: (1) changes in the external shape of particles, or shrinkage; and (2) disintegration of internal structure during oxidation, or fragmentation; and (3) generation of internal micro-pores [27, 49].

1. Shrinkage

Fuel particles undergo significant volume reduction during fixed bed combustion because of ash formation and mass loss in the form of gasification products. Bar-Ziv et al. [27], propose the “Subskeleton” mechanism (shown in the Figure 2.1) to model this shrinking process.

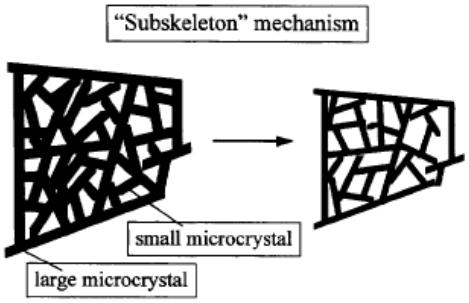

Fig 2.1: The "Subskeleton" mechanism proposed by Kantorovich and Bar-Ziv to simulate shrinkage effects in a fixed bed.
Source: [27]

In the subskeleton model, the structure of the large microcrystal is retained during conversion, while small ones undergo random redistribution in position.

Other shrinkage models proposed by Yang et al. [49] include the shell progressive and ash segregation models. In such models, shrinkage is characterized by its influence on the particle number density and the porosity. Thus, a packing parameter (n) is introduced to assess these phenomena through the relation:

$$(1-\varepsilon) = f_{shrink}^{1-n}(1-\varepsilon_o)$$

Where ε is the bed instantaneous porosity, f_{shrink} is a shrinkage factor defined as the ratio of the instantaneous solid phase volume to the initial solid volume, or

$f_{shrink} = \frac{V_p}{V_{p,o}} = \left(\frac{d_p}{d_{p,o}}\right)^3$, ε_o is the initial bed porosity.

If the packing factor (n) is unity, the porosity does not change. Then, the particle shrinkage results in changes in the particle number density and, subsequently, the bed height. If it is zero, then the shrinkage leads to an increase in porosity. Thus, the density and the bed height do not change [49]. Cooper et al. [55] used a fixed bed combustion model in which shrinkage results in changes in the particle number density only. They

modeled this change by taking horizontal slices of the bed and writing a particle number density (N_P) as:

$$\frac{\partial \mathrm{N_P}}{\partial t} = -\frac{\partial \dot{\mathrm{N}}_\mathrm{P}}{\partial x}$$

$$\Rightarrow \frac{\partial}{\partial t}\left[\frac{(1-\varepsilon)\rho_s}{m_\mathrm{P}}\right] + \frac{\partial}{\partial x}\left[\frac{\rho_s v_s}{m_\mathrm{P}}\right] = 0$$

Where ε is the bed porosity, ρ_s is the solid phase density, m_P is the particle mass, v_s is the superficial velocity of the solid particles.

The above equation is solved for m_P at each time step to account for shrinkage mass loss. The value of $\rho_s v_s$ is obtained from solving the solid mass continuity equation presented before.

2. Fragmentation

Fragmentation is defined as the disintegration of the internal structure of solid fuels during combustion. In other words, fuel particles break into fragments during fixed bed gasification. Fragmentation leads to an increase in the number of particles in the bed (of the second order with time). This increase may be modeled as [60]:

$$\frac{N}{N_0} = 1 + A_1\frac{t}{t_b} + A_2\left(\frac{t}{t_b}\right)^2$$

Where N is the instantaneous number of particles, N_0 is the initial number of particles, A_1 and A_2 are experimental constants (not determined for charcoal yet), t_b is the burnout time for the bed.

3. Generation of Internal Pores

Generation of internal pores is defined as the evolution of mass voidages within the internal bulk of solid particles in the process of fixed bed combustion. This phenomenon is characterized by the appearance of an internal pore fraction (ε_{ip}) which is distinct from the initial porosity fraction, ε. The internal pore fraction is defined for the pores that are generated during the combustion and to be discriminated from the pores that are present in the initial solid fuel. Yang et al. [49] give the definition of ε_{ip} as:

$$\varepsilon_{ip} = \frac{V_{ip}}{V_s}$$

Where V_{ip} is the volume occupied by the internal pores formed during combustion, V_s is phase, the volume of the solid.

Internal porosity generation and dynamics are modeled by a transport equation since these internal pores move along through the advection of the solid phase. The transport equation is analogous to the solid component's conservation law. Thus, according to Yang et al. [49]:

$$\frac{\partial(1-\varepsilon)\varepsilon_{ip}}{\partial t} + \frac{\partial v_s \varepsilon_{ip}}{\partial y} = -\sum_i f_{ip.i} \frac{\dot{\mathrm{M}}_{s,i}}{\rho_{s,i}} + \dot{\varepsilon}_{ip,loss}$$

Where ε is the bed porosity fraction, v_s is the Darcean velocity of solid particles, $\sum_i$ is a summation over all the solid species, $f_{ip,i}$ is the internal porosity factor for solid species i (tendency of species i to form internal pores), $\dot{\mathrm{M}}_{s\to g}$ is the mass rate of change of solid fuel

to gaseous products (gasification), $\rho_{s,i}$ is the density for the ith solid species, $\dot{\varepsilon}_{ip,loss}$ is the rate of loss of internal pore structures by the action of ash segregation.

I. Ash Modeling

Ash forms because of the incombustible mineral components of solid fuels. Ash physical properties are very different from those of the fuel. Thus, the appearance of ash can significantly affect the combustion process occurring in a packed bed. Ash appears as a distinct species in solid conservation processes. However, the most dramatic effects occur in the overall heat and mass transfer phenomena.

Ryan et al. [15] suggest that when ash forms, the solid phase will be composed of an ash and a fuel portion. Thus, they conclude that the mass of ash formed must be balanced by an equal loss in the mass of the fuel. Consequently, they define two mass fractions for the solid phase: Y_A, the ash mass fraction and Y_F, the fuel mass fraction. If fuel particles of initial ash fraction α and diameter $d_{P,F,0}$ have burned down to $d_{P,F}$ at a certain height in the bed, then the local fuel mass fraction is given by:

$$Y_F = \left[1 + \frac{\rho_F}{\rho_A} \alpha \left(\frac{d_{P,F,0}^3}{d_{P,F}^3} - 1 \right) \right]^{-1}$$

Where ρ_F is the fuel density, ρ_A is the ash density.

The fuel particle diameter, $d_{P,F}$, is determined by solving the transport equation for the particle mass, $m_{P,F}$, given by:

$$\frac{\partial}{\partial t}\left(\frac{\rho_F \mathrm{X}_F(1-\varepsilon)}{m_{\mathrm{P},F}}\right)+\frac{\partial}{\partial x}\left(\frac{\rho_F w(1-\varepsilon)Y_F}{m_{\mathrm{P},F}}\right)=0$$

The solids continuity equation may be adjusted to include the effects of ash:

$$\frac{\partial}{\partial t}\left[(1-\varepsilon)\rho_s\right]+\frac{\partial}{\partial x}\left(\rho_F Y_F+\rho_{\mathrm{A}}(1-Y_F)\right)w(1-\varepsilon)=\dot{\mathrm{M}}_{s\to g}$$

Where ε is the overall bed porosity, ρ_s is the averaged solid phase density, ρ_F is the fuel density (excluding ash), Y_F is the fuel mass fraction within the solid phase, ρ_A is the ash density, w is the actual velocity of the fuel and ash downwards, $\dot{\mathrm{M}}_{s\to g}$ is the mass rate of change of solid fuel to gaseous products (gasification).

The ash layer forms a shield that hinders heat transfer from the bed to the surroundings. Thus, the fuel portion of the solid phase will conduct and radiate heat differently. Ryan et al. [15] propose a modified effective thermal conductivity to include the insulating effect of the ash layer:

$$k_{eff}=\frac{V_F\beta}{\gamma/k_F+1/\left(k_g/\phi+d_{\mathrm{P},F}h_{rs}\right)}+(1-V_F)(1-\chi_{\mathrm{A}})d_{\mathrm{P},F}\beta h_{r\upsilon}+(1-V_F)\chi_{\mathrm{A}}k_{\mathrm{A}eff}$$

Where V_F is the fuel volume per unit bed, k_F is the thermal conductivity of the fuel portion of the slid phase, k_g is the gas phase thermal conductivity, $d_{P,F}$ is the fuel particle diameter, χ_{A} becomes unity as the fuel void completely fills with ash, and it remains unity as further ash accumulates and separates the fuel particles, $k_{A,eff}$ is the ash effective thermal conductivity. The other symbols are defined in Yagi et al [62].

Ryan et al. [15] suggest using the thermal conductivity of ash as being equal to that of firebrick, or 1.09 W/m.°K.

J. Chemical Reactions

Carbon oxidation (or combustion) is one of the most important chemical reaction mechanisms known. It is of central importance in several technological fields like the combustion of coal, and biomass chars [10]. The importance of this reaction is appreciated in the sense that coal combustion provided 26% of the global energy demand and 37% of the world's electricity in the eighties [11]. Despite the central importance of the carbon combustion reaction, and even thought the literature dealing with the chemical kinetics of this reaction mechanism is vast and extensive, no general consensus exists about how to model it.

1. Difficulties of Studying the Carbon-Oxygen Reaction

Two types of difficulties arise when modeling carbon combustion: experimental difficulties and theoretical modeling complexities.

a. Experimental Difficulties

The scatter observed in the results of carbon combustion experiments is attributed to different kinds of reasons:

- Absence of general standards for experimental setups and techniques; as well as the methods implemented in interpreting and analyzing the data collected from such experiments [10].
- Significant diversity in the fuels used as the carbon source (graphite, coal, biomass chars). This miscellany of fuels causes considerable divergence in the results of

combustion because of different particle sizes, porosity factors, and impurities contained within fuel samples [10].

- Insufficient knowledge about the morphology of carbonaceous fuels. For example, it is extremely difficult to determine the internal and external areas of carbon as it is burning [12].

- Complications arising from the hydrogen content of carbonaceous fuels. The hydrogen content causes the appearance of radicals such as OH and HO_2. These radicals compete with oxygen to react with carbon. Such a radical action adds significant complexity to the kinetics to the combustion of carbonaceous fuels and leads to inaccuracies in modeling of the oxidation of pure carbon [12].

b. Theoretical Difficulties

Although theoretical and experimental difficulties are interrelated, theoretical modeling obscurities are more complex and serious than experimental ones. Historical disputes have risen about all the aspects involved in theoretical models of carbon combustion because of several limitations:

- Although it has been determined that chemisorption of oxygen onto solid carbon forms the most basic elementary chemical reaction of carbon combustion, many authors do not focus on the kinetics of these surface complexes and adopt semi-global models instead [7, 36-39]. Even among most of the authors who use chemisorption kinetics, there is no consensus regarding the types of these complexes and, accordingly, about the proper oxidation pathways to include in combustion models. Basically different models of carbon-

oxygen complexes with fundamental discrepancies have been proposed. This leaves the chemical modeling of the carbon-oxygen reaction not fully developed yet in terms of the elementary processes of adsorption, desorption, surface complexes formation, and complexes rearrangements [30].

- No agreement exists about the magnitudes of the activation energies and the intrinsic orders involved in both the semi-global models as well as the elementary surface complexes models [10].

The most fundamental question of carbon combustion is whether carbon dioxide is formed as a primary product in the global oxidation reaction (and this remains unresolved). In other words, it is still undetermined whether carbon burns as $C_s + O_2 \rightarrow CO_2$ (one step oxidation from carbon to carbon dioxide) or as $C_s + 1/2\ O_2 \rightarrow CO \quad + 1/2\ O_2 \rightarrow CO_2$ (CO plays a role in the oxidation). This point is the most complex issue of carbon combustion and it has been extensively debated [12, 16, 31, 40, 43, 44, 46, 47, 48]. It is a dispute of such essential importance in the sense that if it were to be resolved, the pathways that successively convert solid carbon to gaseous products would be precisely determined and a comprehensive combustion model would be, then, within reach.

Each of the above theoretical difficulties will be outlined in the next sections.

2. Models of the Carbon-Oxygen Reaction Mechanism

Many authors have proposed different reaction mechanisms to describe carbon combustion. As mentioned previously, the literature dealing with carbon-oxygen reactions is voluminous and thus a comprehensive review on this topic is out of the context of this

paper. However, it is intended here to present a preliminary review of the work of several authors in this aspect.

a. Global Power Kinetics Model[10]

This is the most basic and simplest model that describes the carbon oxygen reaction. To describe how carbon oxidizes, this model features the following chemical reaction:

$$C + O_2 \rightarrow CO / CO_2$$

This means that the global power model assumes that solid carbon reacts with oxygen to form carbon dioxide and carbon monoxide directly. The model thus presents a single step, global, heterogeneous reaction between solid carbon and gaseous oxygen. The rate of the above chemical reaction is given as a simple n^{th} power form given by:

$$r_{gas} = k\ P_{O_2}^n$$

Where: r_{gas} is the overall rate of gasification, k is the reaction rate constant, P_{O_2} is the oxygen partial pressure. The global power kinetics model is entirely empirical and cannot be derived from elementary reactions. This model has limited utility. It may find some practical use in modeling pulverized fuel combustion that takes place at a temperature range of 1500°K to 2000°K.

b. Semi-global Models

These models are more detailed than the global power kinetics model in the sense that they introduce intermediate reactions for carbon monoxide formation. However, semi-

global models do not include the elementary chemical reactions of carbon-oxygen surface complexes. Several authors propose different forms of these models.

Gremyachkin, Fortsch, Schnell, and Hein [33] developed a theoretical model for the combustion of a porous carbon particle. Gremyachkin et al. adopt the following model for carbon oxidation:

- Heterogeneous chemical reactions:

  1) $C + O_2 \rightarrow CO_2$

  2) $2C + O_2 \rightarrow 2CO$

  3) $C + CO_2 \rightarrow 2CO$ (The "Boudouard Reaction")

- Homogeneous chemical reaction:

  4) $2CO + O_2 \rightarrow 2CO_2$

The heterogeneous reactions occur on the exposed carbon surfaces (either inside the porous carbon particle or at the exterior surface). The homogeneous reaction takes place in the gaseous phase that is either near the particle or inside the voids of the porous particle.

The rate of reaction 2 is given as [12]:

$$R_2 = 305.[O_2]^{1/2}.e^{\left(\frac{-179kJ/mol}{RT}\right)} \quad [\text{g/cm}^2\text{.s}]$$

The rate of the heterogeneous reaction 3 is given as [34]:

$$R_3 = 760.[CO_2].e^{\left(\frac{-30205}{T}\right)} \quad [\text{kg/m}^3\text{.s}]$$

The rate of the homogeneous reaction 4 is [35]:

$$R_4 = \frac{d[CO_2]}{dt} = 1.05*10^{10}*[CO]*[O_2]^{0.5}*[H_2O]^{0.25}*MW_{CO_2}*e^{\left(\frac{-14293}{T}\right)} \quad [\text{kg/m}^3\text{.s}]$$

Howard et al. [63] propose a rate constant for reaction 4 as:

$$k_4 = 1.3*10^{11}*[CO]*[O_2]^{0.5}*[H_2O]^{0.5}*MW_{CO_2}*e^{\left(\frac{-15105}{T}\right)} \text{ [kmol/m}^3\text{]}$$

Matsui [36] experimentally studied the behavior of the combustion rate of carbon when the flame sheet attaches or collapses at the carbon surface. In this study he uses a model that features semi-global chemical reactions. Matsui uses a model that is composed of two heterogeneous chemical reactions for the gasification of solid carbon:

$$1)\ 2C_s + O_2 \rightarrow 2CO_2$$

$$2)\ C_s + CO_2 \rightarrow 2CO$$

The above reactions are complemented by the homogeneous reaction of carbon monoxide oxidation:

$$3)\ CO + O_2 \rightarrow CO_2$$

Some authors extend the above reaction mechanism to include the reaction of water vapor (humidity in air) with solid carbon as:

$$4)\ C_s + H_2O \rightarrow H_2 + CO$$

Matsui theoretically formulates the overall dimensionless rate of carbon oxidation as:

$$-f_w = \frac{1}{\left(\frac{MW_{O_2}}{2MW_C}\right).\left(\frac{2MW_{CO_2}}{MW_{O_2}}\right)}\left[335000\,.\tilde{Y}_{O_2}.e^{\left(-\frac{3.49*5164}{T_w}\right)} + 9500\,.\tilde{Y}_P.e^{\left(-\frac{4.08*5164}{T_w}\right)}\right]$$

Where MW is the molecular weight of the species shown in the subscript, T_w is the temperature of the carbon surface, $\tilde{Y}_{O_2}$ is a dimensionless form of the oxygen mass fraction,

$$\tilde{Y}_P = \frac{\left(\tilde{Y}_{O_2,\infty}\right)\left(\frac{MW_{O_2}}{MW_C}\right)\left(\frac{2MW_{CO_2}}{MW_{O_2}}\right)}{2\left(\frac{MW_{O_2}}{MW_C}\right)\left(\frac{2MW_{CO_2}}{MW_{O_2}}\right)+2\left(\tilde{Y}_{O_2,\infty}\right)}$$

Libby and Blake [37] used the latter semi-global carbon oxidation model to investigate the dynamic behavior of single carbon particles in a hot oxidizing ambient. They assumed constant density, uniform temperature, spherical carbon particles. Libby and Blake concluded that both direct carbon oxidation (equation 1) and indirect oxidation (equation 2) play a significant role in the dynamic behavior of carbon combustion. In another study [14], these authors developed a theory that describes the behavior of carbon particles in a slow viscous flow of oxidizer. They combined equations 1 and 2 of the semi-global model with the concept of a flame sheet.

Mantalon and Moshe [38] studied the rate of mass loss of a pure carbon particle by observing the dynamics of the gas phase (mainly reaction 3). They assumed the existence of a flame sheet in which the total oxidation of CO occurs (which may assume different positions according to the flow conditions). When the flame sheet stands adjacent to the carbon particle, oxygen is in excess and the mass loss rate depends on both reactions 1 and 2. On the other hand, when the sheet exists at a distance from the particle oxygen does not reach the particle and the mass loss rate depends on indirect oxidation (reaction 3) only.

Adomeit, Hocks, and Henriksen [39] theoretically investigated the combustion behavior of a carbon surface exposed to the stagnation flow of a moist oxidizer. They used an extended semi-global model that consists of the three previously stated equations 1, 2, and 3; in addition to the hydroxyl radical interactions. They calculated the reaction rates of

the homogeneous reactions of this extended model for finite rate cases and for the limiting cases of frozen and infinitely fast reactions. For various combinations of oxygen and humidity mass fractions, they concluded that the Boudouard reaction is relatively slow especially in the range of 1200-2000°K. In this temperature range, Adomeit et al. realized that the overall combustion rate decreased with an increase in the in the humidity of the flow. This decrease is due to the acceleration of the homogeneous reactions by small amounts of water vapor (occurring only in the case of a slow Boudouard reaction). From various combinations of the flow conditions they showed that the usual trends of studying the limiting cases of the homogeneous reactions can not reproduce the exact combustion rates. They propose a full description of the interactions of the chemical and transport processes in order to precisely determine the combustion kinetics of carbon.

Borman [7] explains char fixed bed combustion modeling and proposes the use of the semi-global model with the addition of the reaction of water vapor with solid carbon (reaction 4).

c. Surface-Complexes Semi-Global Models

These models include the kinetics of chemisorption of oxygen onto carbon surfaces. When oxygen is brought in close contact with carbon, oxygen particles start to chemically adsorb onto the carbon atoms forming what is known as a carbon-oxygen complexe. Surface oxygen complexes were first discovered by Walker [40].

Some authors believe that only elementary oxygen adsorbs onto carbon forming C(O). Others add molecular oxygen adsorption $C(O_2)$. Consequently, several surface-complexes models have been proposed.

The Langmuir-Hinshelwood kinetics [10] model carbon combustion using two step semi-global chemical reactions. In this model, the carbon-oxygen complex forms gaseous CO.

The Langmuir-Hinshelwood model features the following chemical reactions:

$$1)\ C + O_2 \rightarrow C(O)$$

$$2)\ C(O) \rightarrow CO$$

The first of the above two equations presents oxygen adsorption onto solid carbon. The second reaction is the desorption of the C (O) complex thus forming gaseous CO. The activation energy of adsorption ranges from 10 to 125 KJ/mol, while that of desorption ranges from 160 to 400 KJ/mol. The overall gasification rate is given by:

$$r_{gas} = \frac{k_1 k_2 P_{O_2}}{k_1 P_{O_2} + k_2}$$

Where: r_{gas} is the overall rate of gasification, k_1 and k_2 are the first and second reaction rate constants respectively, P_{O_2} is the oxygen partial pressure. The Langmuir-Hinshelwood model exhibits two limiting cases:

- Low temperatures ($k_2 << k_1$), then $r_{gas} = k_2$. This implies zeroth order (in oxygen) and desorption control.
- High temperatures ($k_1 << k_2$), then $r_{gas} = k_1 P_{O_2}$. This implies first order (in oxygen) and adsorption control.

The above limiting cases are the exact opposite of the expected trend (high order in low temperature ranges, and low order at elevated temperatures). In this sense, many authors have described the Langmuir-Hinshelwood model as an “empirical expression that

contains an additional parameter to allow a variable reaction order within a given data set" [10]. The Langmuir-Hinshelwood model's utility is limited to certain temperature ranges and oxygen concentrations.

Marsh and Kuo [41], propose a reaction mechanism consisting of the following elementary chemical reactions:

$$C_s + O_2 \rightarrow C(O_2) / C(O_2)_m$$

$$C(O_2)_m \rightarrow C(O) + C(O_2)_m \, or \;\; C(O)_m + C(O_2)_m \, or \;\; C(O) + C(O_2)$$

$$C(O)_m \rightarrow CO$$

$$C(O)_m + C(O)_m \rightarrow C_s + CO_2$$

$$C(O)_m + C(O) \rightarrow C_s + CO_2$$

$$CO + C(O) \rightarrow C_s + CO_2$$

$$CO + C(O)_m \rightarrow C_s + CO_2$$

$$O_2 + 2C(O) \rightarrow 2CO_2$$

Where $C(O_2)_m$ is a molecular oxygen mobile surface complex, $C(O)_m$ is an atomic oxygen mobile surface complex.

Atamny, Blocker, and Dubotzky [42] propose the following reaction mechanism:

$$C_b + 1/2 \; O_2 \rightarrow 1/2 \; C(O_2)_m$$

$$C(O_2)_m \rightarrow C(O)_m$$

$$C(O)_m + C_e \rightarrow C(O)$$

$$C(O) + C_b \rightarrow CO + C_e$$

$$C(O) + C(O)_m \; or \; C(O) \rightarrow CO_2 + 2C_e \; or \; CO_2 + C_e + C_b$$

Where C_b is free carbon basal site, C_e is a carbon active edge site, $C(O_2)_m$ is a molecular oxygen mobile surface complex, $C(O)_m$ is an atomic oxygen mobile surface complex.

Ahmed, Back, and Roscoe [43] experimented on thin films of carbon and using temperature programmed oxidation to study the nature and role of surface complexes that form during temperature carbon gasification. They categorized two types of surface carbon-oxygen complexes. These two are the slow and the fast carbon-oxygen complexes. Their reaction mechanism can be represented by the following minimum set of reactions:

1) $C_{fast} + O_2 \rightarrow C(O_2)_{fast}$

2) $C_{fast} + C(O_2)_{fast} \rightarrow 2C(O)_{fast}$

3) $C(O)_{slow} \rightarrow CO + C_{slow}$

4) $C_{slow} + O_2 \rightarrow C(O_2)_{slow}$

5) $C_{slow} + C(O)_{slow} + O_2 \rightarrow CO_2 + C(O)_{slow} + 2C_{slow}$

6) $C_{slow} + C(O)_{slow} + O_2 \rightarrow CO_2 + C(O)_{slow} + C_{slow}$

7) $C_{slow} + C(O)_{fast} + O_2 \rightarrow CO_2 + C(O)_{slow} + C_{fast}$

8) $C_{slow} + C(O_2)_{fast} \rightarrow C(O)_{fast} + C(O)_{slow}$

Table 2.1: The kinetic parameters used in the carbon combustion model proposed by Ahmed et al.
Source: [43]

Reaction	Ea [kJ/mol]	Ln A	K
1	50	13.9	$700/ASC_A$ [1/s]
2	190	28.3	$0.64/ASC_B$ [1/s]
3	110	24.3	$2800\ /ASC_A$ [1/s]
4	270	29.9	$1.5*10^{-5}$ [1/s]
5	270	56.9	$1.6*10^{7}\ /ASC_B$ [1/mol.s]
6	150	43.3	$8*10^{8}\ /ASC_B$ [1/mol.s]
7	33	24.2	$1.4*10^{8}\ /ASC_B$ [1/mol.s]
8	170	32.9	$1.1*10^{3}\ /ASC_B$ [1/s]

ASC is defined as the total moles of active surface carbon (for type A and type B sites according to the subscript). The mathematical expression for ASC is explained by Laine et al. [64]. Ahmed et al. measured ASC_A and ASC_B to be equal to $5.3 * 10^{-7}$ moles of carbon for the graphite used in their experiments.

Du, Sarofim, Longwell, and Mims [44] studied carbon adsorption/desorption properties during soot oxidation. They proposed an oxidation model similar to that of Ahmed et al. However, instead of the duality of site types suggested by Ahmed et al., they proposed the existence of a range of activation energies possessing two maxima. These activation energies were assumed to have a Gaussian distribution. Du et al. experimentally determined the mean and standard deviation of these Gaussian energy profiles for saturated and unsaturated soot. They also gave Arrhenius forms of reaction constants. Du et al. finally reported an order of oxidation of 0.83 with respect to the oxygen partial pressure.

Haynes [45] studied the carbon oxidation reactions by focusing on the role stable C(O) complexes. He examined high temperature carbon oxidations (combustion) and focused only on the CO formation since it is the primary product in typical high-

temperature combustion processes. In other words, Haynes studied the adsorption and then the desorption of C(O) complexes to form CO (mostly) directly. Thus, in order to evaluate the rate of carbon gasification (forming mostly CO), it was sufficient to determine the rate of desorption of C(O) complexes. Haynes uses the following chemical reactions:

$$1)\ C_s + O_2 \rightarrow C(O) + CO$$

$$2)\ C(O) \rightarrow C_s + CO, CO_2$$

$$3)\ C(O) + O_2 \rightarrow C(O) + CO, CO_2$$

To determine the rate of C(O) desorption, Haynes assumed a stochastic description of the population of surface oxides. This means that at any time the C(O) surface complexes have their characteristic activation energy for decomposition (E_{des}) as a stochastic variable. In this sense, the number of surface complexes is a function of E_{des} and time, or $N(E_{des}, t)$. The rate of decomposition of surface oxides is given by:

$$\frac{dN(E_{des})}{dt} = -10^{14}.N(E_{des}, t).e^{\left(\frac{-E_{des}}{RT(t)}\right)}$$

Haynes derived expressions for the steady state number of surface complexes as a function of the stochastic variable $N(E_{des})$, as well as the rate of complex adsorption r_{ads} . These lead to the formulation of an overall gasification rate as:

$$-\frac{1}{w}\frac{dw}{dt} = \left(2MW_C(1-f) + (MW_C - MW_O)f\right)r_{ads} + (MW_C + MW_O)\int_{E_{des}}^{\infty} k_{des}(E_{des}).N(E_{des})dE_{des} + MW_C k_{ox} N_{tot}$$

Where w is the weight of carbon, MW_C and MW_O are molecular weights of carbon and

oxygen, f is a temperature dependant constant, k is a rate constant, N_{tot} is the total number of surface complexes given by $N_{tot}(t) = \int_0^\infty N(E_{des}, t) dE_{des}$.

Li and Brown [31] used temperature programmed oxidation (TPO) to study the kinetics of charcoal and graphite combustion at low oxygen partial pressures. Li and Brown assumed the following model:

$$1)\ C_s + O_2 \rightarrow C(O_2)$$

$$2)\ C(O_2) \rightarrow C(O) + CO$$

$$3)\ C(O) \rightarrow CO$$

$$4)\ C_s + O_2 \rightarrow CO_2$$

$$5)\ C_s + O_2 \overset{C(O_2)}{\rightarrow} CO_2$$

$$6)\ C_s + O_2 \overset{C(O)}{\rightarrow} CO_2$$

Reactions 2 and 3 describe carbon monoxide evolution, while equations 4 and 5 are related to carbon dioxide evolution. Thus, the temperature-rates of evolution of CO and CO_2 may be represented as:

$$\frac{d[CO]}{dT} = \frac{k_2}{H}[C_s]p_{O_2}^{n_2} + \frac{k_3}{H}[C(O)]p_{O_2}^{n_3}$$

$$\frac{d[CO_2]}{dT} = \frac{k_4}{H}[C_s]p_{O_2}^{n_4} + \frac{k_5}{H}[C(O)]p_{O_2}^{n_5}$$

Where H is the heating value of the combustion process (experimentally controlled variable in this case), k is the rate constant corresponding to the reaction number shown in

the subscripts, p_{O_2} is the partial oxygen pressure, and n is the reaction order corresponding to the reaction number shown in the subscripts.

Li and Brown obtained numerical kinetic parameters for the above rate equations. This enabled the quantification of the CO and CO_2 concentrations. The authors thus suggest rate expressions for the ratio CO/CO_2. For example, in the case of granular charcoal of particle sizes ranging between 0.85 and 1.7 mm:

$$CO/CO_2 = 10^{3.5\pm1.5}.P_{O_2}^{-0.8\pm0.13}.e^{\left(\frac{-6700\pm3300}{T}\right)}$$

Hurt and Calo [10] proposed a three-step semi-global model. This model is heavily based on oxygen-carbon chemisorptions. Hurt's model featured the following chemical reactions:

1) $C + O_2 \rightarrow 2C(O)$

2) $C(O) + O_2 \rightarrow CO_2 / CO$

3) $C(O) \rightarrow CO$

Reaction 1 presents oxygen adsorption onto solid carbon. The second reaction represents the reaction between gaseous oxygen and surface complexes ($C(O)$). The third reaction is the desorption of the C(O) complex to form gaseous CO.

The rates of the previous three chemical reactions are given as:

$$R_1 = k_1 P_{O_2} (1-\theta)$$

$$R_2 = k_2 P_{O_2} \theta$$

$$R_3 = k_3 \theta$$

Where: R_1, R_2, R_3 are the rates of reactions 1, 2, and 3 respectively; k_1, k_2, and k_3 are the first, second, and third reaction rate constants respectively; P_{O_2} is the oxygen partial pressure; θ is the fraction of sites occupied by a complex. The above expressions can be combined to obtain the overall gasification rate as

$$r_{gas} = \frac{k_1 k_2 P_{O_2}^2 + k_1 k_3 P_{O_2}}{k_1 P_{O_2} + k_3 / 2}$$

The CO/CO_2 ratio is also given as:

$$CO/CO_2 = \frac{k_3}{k_2 P_{O_2}}$$

Hurt's model exhibits the following trends:

- Low temperatures: k_3 is small, region of oxygen complex reaction control, $r_{gas} = k_2 P_{O_2}$.
- Low-moderate temperatures: $k_3 << k_1 P_{O_2}$, region of mixed desorption-oxygen complex control, $r_{gas} = k_2 P_{O_2} + k_3$.
- Moderate temperatures: $k_2 P_{O_2} << k_3 << k_1 P_{O_2}$, region of desorption control.
- High moderate temperatures: $k_2 P_{O_2} << k_1 P_{O_2} \; and \; k_2 P_{O_2} << k_3$, region of mixed desorption-adsorption.
- Very high temperatures: k_3 is large, region of adsorption control.

It is evident from the above temperature domains that basically there is an oxygen complex control region (low temperatures), followed by a region of desorption control (moderate temperatures), which in turn is followed by a region of adsorption control (high

temperatures). These transitional regions explain the change of global order (as expected) from high orders at low temperatures, to low orders at moderate temperatures, and back to high orders at very high temperatures. It is clearly shown that the model does result in the correct reaction order trends (in Figure 2.2). Hurt's semi-global model accurately predicts carbon combustion for purposes of combustion modeling. Unfortunately, Hurt and Calo do not provide exact numerical Arrhenius parameters for their model. Instead, they use relative rates for the chemical reactions of the model.

3. Carbon-Oxygen Reaction Global Order with respect to Oxygen

In spite of the vast disagreement about the kinetics of the carbon-oxygen reaction, several reviews have found some general trends in the reported global reaction order (with respect to oxygen). For example Smith I.W. [13] has summarized the kinetics of coal char oxidation. On the other hand, Hurt R.H. and Calo J.M. [10] have reviewed many new studies and concluded that there exists evidence for clear trends in reporting kinetic parameters for the carbon oxidation reaction. This discussion is mainly a review of their findings.

The order of the carbon-oxygen reaction is temperature dependant. There are three distinct zones along the temperature scale that are known to demonstrate different magnitudes of the intrinsic order. Figure 2.2 shows these three zones clearly. These zones will be labeled as: Zone I (temperatures less than 900°K), Zone II (temperatures between 1100°K and 1700°K), and Zone III (temperatures above 1600°K).

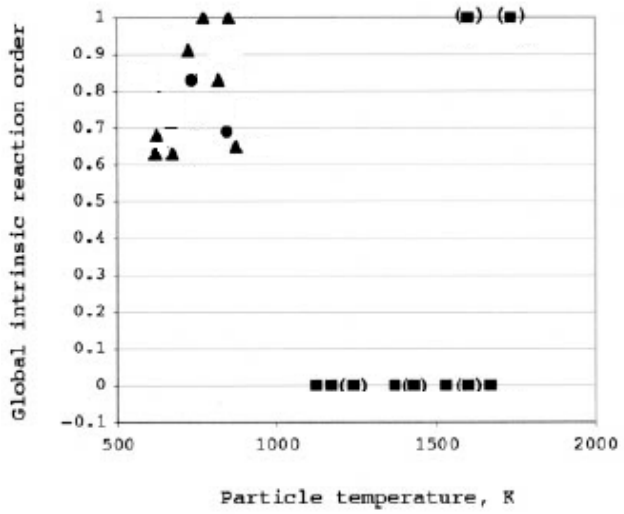

Fig 2.2: Compilation of Global Intrinsic Reaction Orders for the Carbon-Oxygen Reaction
Source: [10]

a. Zone I

Zone I corresponds to carbon oxidation reactions that take place at temperature values that are less than 900°K. This temperature range is typical of char combustion that occurs in small stoves. Zone I features high fractional order that varies between 0.6 and unity. Most of the studies that were carried out in this temperature range have implemented thermogravimetry and directly measured the order of the carbon-oxygen reaction.

b. Zone II

Zone II corresponds to studies of the carbon-oxygen reaction that focused on a temperature range between 1100°K and 1700°K. Fluidized bed combustion (of char) is associated with this temperature range. In addition, industrial grates and kilns operate within the temperature limits of Zone II. The global order in this zone seems to fall from unity to zero. This decrease in the magnitude of the order is an imperative feature in the

kinetics of the carbon-oxygen reaction. Consequently, it is highly crucial for any proposed model for carbon oxidation to precisely account for this decreasing trend.

c. Zone III

Zone III corresponds to carbon oxidation that occurs above 1600°K. The intrinsic order of such an oxidation is believed to be unity in this regime. The carbon-oxygen reaction is adsorption controlled in Zone III. This explains the abrupt global order increase that occurs above 1500°K. Again, a proper carbon oxidation model must account for this increasing trend that takes place at high temperatures.

4. Debate on whether CO_2 is a Primary Product

One of the most challenging aspects of the carbon oxygen reaction lies in this question: does carbon react with oxygen to produce CO_2 directly or is CO produced first and then this CO eventually oxidizes to CO_2? Carbon monoxide is a primary product of carbon oxidation for sure, but is carbon dioxide a primary product as well? This has been and continues to be debated by many authors. Several argue that CO_2 is a primary product. For example, Vastola, Hart, and Walker [46] studied carbon oxygen surface complexes using O^{18} as a tracer to evaluate the extent to which the desorption of C(O) contributes to the evolution of CO and CO_2. They concluded that upon the reaction of carbon with oxygen, CO, CO_2, and a carbon-oxygen surface complex form. They argued that primary CO_2 is formed via chemical interaction between two carbon-oxygen complexes as:

$$C(O)+C(O)\rightarrow CO_2+C_s$$

Marsh and Foord [47] suggest that primary CO_2 is also formed when gaseous species interact with the surface complexes. Thus, they add to the above reaction an additional path for the evolution of primary CO_2.:

$$C(O) + CO \rightarrow CO_2 + C_s$$

Ahmed and Back [43] argue that primary CO_2 is formed from the chemical interaction between the molecular oxygen complex and the oxide complex as:

$$C(O) + C(O_2) \rightarrow CO_2 + C(O)$$

They also suggest that interactions of free carbon sites with stable complexes and oxygen produce primary CO_2 as:

$$C_s + C(O) + O_2 \rightarrow CO_2 + C(O) + 2C_s$$

Brown, Lear, and Haynes [48] studied oxygen chemisorption on carbon over wide ranges of temperature and oxygen partial pressure. They concluded that primary CO_2 is formed when gaseous oxygen reacts with molecular surface complexes as:

$$C(O_2) + 1/2\ O_2 \rightarrow CO_2 + C(O)$$

Du, Sarofim, Longwell, and Mims [44] experimented on the oxidation kinetics of catalyzed and catalyzed soot and concluded that primary CO_2 is formed on a small number of sites. They argue that a chemical interaction of a fixed carbon site with gaseous oxygen yields primary CO_2. This mechanism is the same as the global power kinetics model:

$$C_s + O_2 \rightarrow CO_2$$

Walker, Taylor, and Ranish [40] agree with the above path but suggest that primary CO_2 may be formed from an additional path that involves the interactions of surface chemisorptions as:

$$C(2O) \rightarrow CO_2$$

CHAPTER 3

MODEL AND EXPERIMENTS DESCRIPTION

A. Smoking Topography Description

Smoking topography is a description of when and how long a smoker inhales (takes a puff) as well as when and how long does the smoker rests between puffs. It also describes how much smoke is inhaled at each puff. In other words, a smoking topography is a quantification of the following parameters:

- Puff duration: the time of the inhaling period (how many seconds are spent during one puff).
- Puff flow rate: this is the volume (or mass) flow rate that enters a smoker's mouth during puffing.
- Interpuff interval: this is the amount of time a smoker spends between two successive puffs.

A real smoking topography is stochastic in the sense that it is characterized by variable and random puff durations, puff flow rates, and interpuff intervals. However, a stochastic smoking pattern could be represented by an equivalent periodic pattern. This conversion must retain the same net displaced volume, average puff duration, average interpuff interval, and number of puff events.. Figure 3.1 shows a comparison between a typical stochastic and an equivalent periodic smoking session.

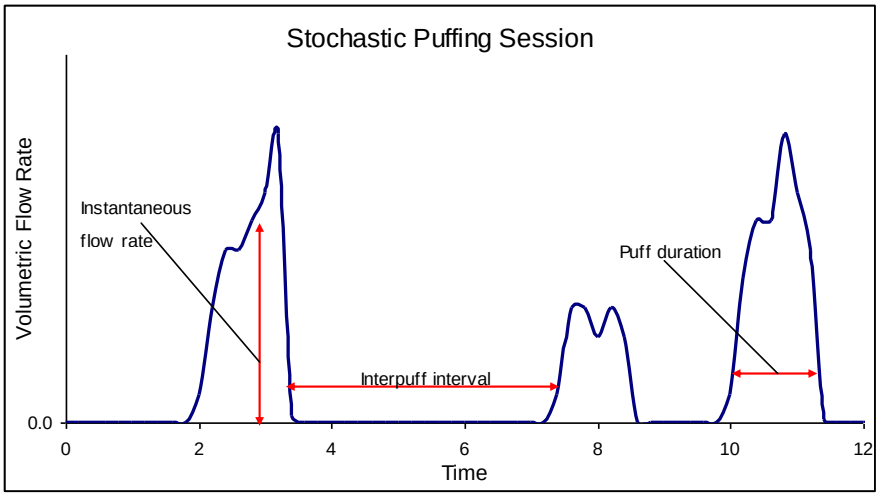

Fig 3.1: Typical smoking topography for a real life smoking session.

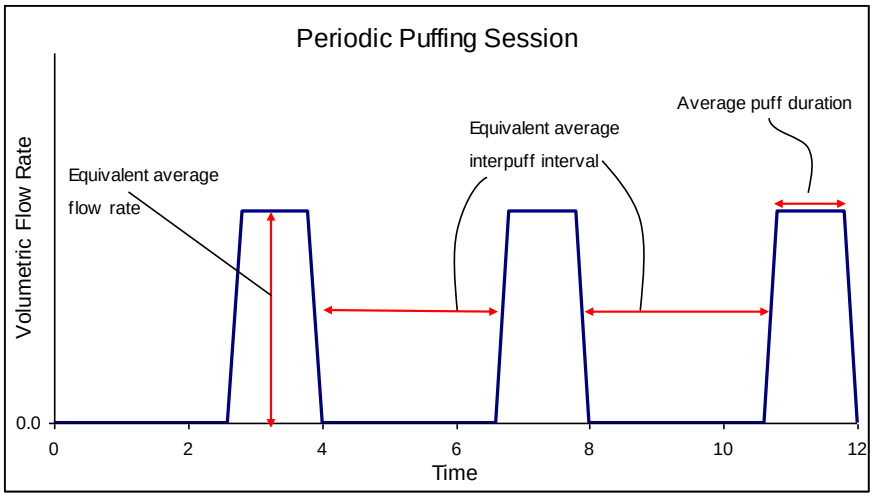

Fig 3.2: Smoking topography for a steady periodic smoking session.

B. Model Description

The combustion of charcoal on a narghile head is properly modeled by fixed bed combustion. Thus, the basic model in this work will be a fixed bed of porous carbon through which a time-varying flow of air is forced. The main goal would be to compute the resulting CO exiting the bed for two puffing (ventilation) conditions: steady periodic, and

random. Both puffing topographies will have the same net volume flow, average interpuff interval, and number of puff events (for them to be considered equivalent).

The physical laws that govern fixed bed combustion (explained in the "background" section) will be applied to the charcoal in order to arrive at a computational model for this combustion process. In order to model charcoal fixed bed combustion, it will be subdivided into several elements of depth dx as shown in Figure 3.3. Conservation equations will be solved in each element. Thus, a time-marching solution of the temperature and the species mass fractions will be obtained.

The mass and energy conservation laws that govern the combustion process of the charcoal lead to a system of partial differential equations. In general, the independent variables are time and the three spatial coordinates. However, it is proposed that the charcoal fixed bed combustion model will be solved in one dimensional space. In the end, the main interest of this study is the system dynamic behavior subject to a random versus periodic forcing function, rather than resolving the details of the char. For this purpose, it is sufficient to use a one dimensional formulation, particularly since the reduced computations will afford the opportunity to run longer simulations.

In order to allow for efficient computation times, other justifiable assumptions will be made. These assumptions are:

- The radiation within the fixed bed is neglected. This is because the magnitude of heat transfer by radiation is small compared to other modes of heat transfer (conductive and convective) and to the heat release by exothermic chemical reactions.

- The solid phase retains a constant void fraction, mean particle diameter, and density as it burns. In reality, various physical changes occur within the fuel bed (explained previously).

- Pressure drop though the char bed is neglected.

- The char bed is perfectly insulated, and thus it does not loose heat to its surroundings except at the outlet which is maintained at a fixed boundary temperature. In reality the char surface will lose heat to the surrounding medium via convection and radiation.

- The kinetic energy of the flowing gas phase will be neglected. The value of this kinetic energy is negligible compared to the energy transport processes (conductive and convective) and to the energy of heat release (from exothermic chemical reactions).

- The specific heat values (gas and char) will be taken as a constant since they only change slightly over the temperature range of interest. In a comprehensive study, Larfeldt et al. made a comparison between using constant versus temperature dependant specific heat values. They recommended that it is best to use a constant average value of 1000 J/Kg. °K. The reason behind this is that the temperature dependences of the thermal conductivity and that of the specific heat cancel each other.

- Infinite heat transfer between the gas and solid phases. This means that the temperature of the solid is equal to that of the gas phase at any point inside the bed. In other words, there will be no need to write separate energy equations for the gas and the solid phased (only one energy equation is sufficient). This assumption is explained by the fact

that air flow within the highly porous charcoal is a 'tortuous' flow. In this sense, air and char are considered in thermal equilibrium throughout the combustion process.

The previous assumptions lead to the development of a fixed bed combustion model. This model is features the mass and energy conservation equations. Following is an explanation of the derivation of these equations for the charcoal bed in hand.

1. Mass Conservation

The general expression of the vector form for mass conservation of a given species (*i* th species) is given by:

$$\frac{\partial(\rho Y_i)}{\partial t} + \nabla.\dot{m}_i'' = \dot{m}_i'''$$

For the charcoal burning model, the following conditions can be applied:

- Assume that the flow is one dimensional (x-coordinate only)

$\Rightarrow \nabla.\dot{m}_i'' = \frac{d}{dx}(\dot{m}_i'')$.

- $\dot{m}_i'''$ is the mass production rate of species i (per unit bed volume). The expression of $\dot{m}_i'''$ is given by $\dot{m}_i''' = MW_i * \dot{w}_i$.

Given the above conditions and assumptions, the previous equation can be rewritten as:

$$\frac{\partial(\rho Y_i)}{\partial t} + \frac{d}{dx}(\dot{m}_i'') = MW_i * \dot{w}_i$$

Where: ρ is the density of the gaseous phase (air flowing within the charcoal). Y_i is the mass fraction of the species i in the gaseous phase. t is time. x is the spatial coordinate.

$\dot{m}_i''$ is the mass flow rate of species i of the gaseous phase (per unit bed area). MW_i is the molecular weight of species i of the gaseous phase. $\dot{w}_i$ is the production rate of species i of the gaseous phase.

The reactive species present in the gaseous flow are water vapor, carbon dioxide, carbon monoxide, and oxygen. Thus, the above equations develop into a set of four partial differential equations (one for each of the reactive species). These are:

$$\frac{\partial\left(\rho_{mix}Y_{H_2O}\right)}{\partial t}+\frac{d}{dx}\left(\dot{m}''_{H_2O}\right)=MW_{H_2O}*\dot{w}_{H_2O} \qquad (1)$$

$$\frac{\partial\left(\rho_{mix}Y_{CO_2}\right)}{\partial t}+\frac{d}{dx}\left(\dot{m}''_{CO_2}\right)=MW_{CO_2}*\dot{w}_{CO_2} \qquad (2)$$

$$\frac{\partial\left(\rho_{mix}Y_{CO}\right)}{\partial t}+\frac{d}{dx}\left(\dot{m}''_{CO}\right)=MW_{CO}*\dot{w}_{CO} \qquad (3)$$

$$\frac{\partial\left(\rho_{mix}Y_{O_2}\right)}{\partial t}+\frac{d}{dx}\left(\dot{m}''_{O_2}\right)=MW_{O_2}*\dot{w}_{O_2} \qquad (4)$$

In the current model, the above equations will be further simplified according to the pseudo transient model described later.

2. Energy Conservation

In order to model energy balances within the burning bed of char, we will divide the char into layers of uniform temperatures. Figure 3.4 shows one layer with its two neighboring layers (above and beneath). The three layers are characterized by their temperatures (To, T_1, and T_2). The energies associated with the layer are:

- The energy of the gas convection ($\dot{Q}_{conv,in,gas}$ and $\dot{Q}_{conv,out,gas}$).

- The energy of the gas conduction ($\dot{Q}_{cond,in,gas}$ and $\dot{Q}_{cond,out,gas}$).
- The energy of the solid conduction ($\dot{Q}_{cond,in,Solids}$ and $\dot{Q}_{cond,out,Solid}$).
- The energy generated due to chemical reactions in the solid and in the gas phases ($\dot{Q}_{Solid}$ and $\dot{Q}_{gas}$).

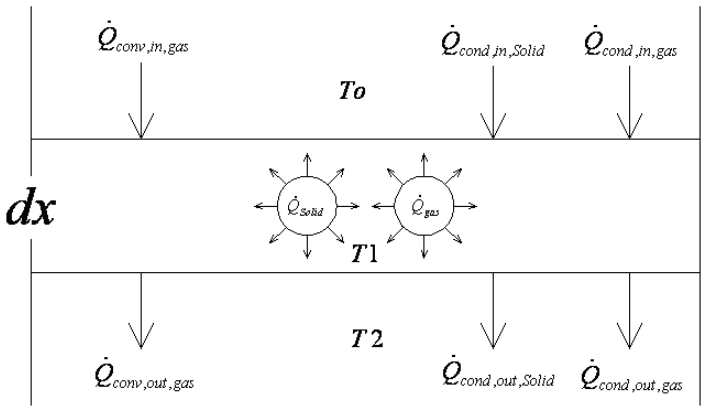

Fig 3.3: Heat conduction, convection, and generation within the fixed bed.

Writing the first law of thermodynamics for the control volume shown in Figure 3.4 (layer with temperature T_1), we get

$$\frac{dE}{dt} = E_{in} - E_{out}$$

$$\Rightarrow (\rho_{bed} C_{bed}) \frac{dT}{dt} = \left(\dot{Q}_{conv,in,gas} - \dot{Q}_{conv,out,gas}\right) + \left(\dot{Q}_{cond,in,gas} - \dot{Q}_{cond,out,gas}\right) + \left(\dot{Q}_{cond,in,Solid} - \dot{Q}_{cond,out,Solid}\right) + \left(\dot{Q}_{gas} + \dot{Q}_{Solid}\right)$$

We note that $\dot{Q}'''_{TOT}$ is the total heat released by chemical reactions (gas and solid), and that $\dot{Q}'''_{TOT} = \sum h^o_{f,i} \dot{w}_i$, thus the energy equation becomes:

$$(\rho_{bed} C_{bed}) \frac{dT}{dt} = -\left(\dot{m}''_{mix} \varepsilon C_P \frac{dT}{dx}\right) + \left(\left[k_{gas}(\varepsilon) + k_{Solid}(1-\varepsilon)\right] \frac{d^2T}{dx^2}\right) + \left(\sum h^o_{f,i} \dot{w}_i\right) \qquad (5)$$

Where: ρ_{bed} is the density of the bed fuel material (charcoal). C_{bed} is the specific heat of the fuel material. T is the temperature. $\dot{m}''_{mix}$ is the mass flow rate of the gaseous mixture (per unit bed area). ε is the fuel bed porosity factor. C_P is the specific heat of the gaseous phase. k_{gas} is the thermal conductivity of the gas phase. k_{Solid} is the thermal conductivity of the fuel solid phase. $h^o_{f,i}$ is enthalpy of formation of the species i (of the gas phase). $\dot{w}_i$ is the production rate of species i of the gaseous phase.

3. Chemistry

The conservation laws contain species production rates (given on a molar basis as $\dot{w}_i$). These values need to be determined from laws that govern the rates of production/destruction of species. This is where chemical reactions enter the scene.

Charcoal is mostly composed of carbon (60-95% by weight). In essence, the chemical modeling of charcoal combustion reduces to that where solid carbon is oxidized to yield carbon-oxygen products (CO_2 and CO).

The carbon combustion model in this work features a three step chemical mechanism. These are:

$$C_{(s)} + \frac{1}{2}O_2 \rightarrow CO \ldots\ldots\ldots \Re_1 \text{(For the } C \text{, (char) oxidation process)}$$

$$CO + \frac{1}{2}O_2 \rightarrow CO_2 \ldots\ldots\ldots \Re_2 \text{(For the } CO \text{ oxidation process)}$$

$$C_{(s)} + CO_2 \rightarrow 2CO \ldots\ldots\ldots \Re_3 \text{(For the } CO_2 \text{ reduction process)}$$

In the above chemical model, it is noticed that:

Reaction 1 is a heterogeneous reaction involving solid carbon reacting with gaseous oxygen to yield carbon monoxide. Reaction 2 is a homogeneous reaction of carbon monoxide oxidation to yield carbon dioxide. Reaction 3 is a heterogeneous reaction that reduces carbon dioxide to carbon monoxide.

The rates of the three reactions given in the above model are given by:

$$\Re_1 = \frac{-12*6*(1-\varepsilon)*\rho_{O_2,\infty}}{16*d*\varepsilon*MW_C*\left(\frac{1}{52.3*T*e^{\left(\frac{-9645}{T}\right)}}+\frac{1}{d*\Phi*D_{O_2-char}*\left(2+0.6\,\mathrm{Re}_d^{1/2}\,Sc^{1/3}\right)}\right)}$$

[9]

$$\Re_2 = \frac{d[CO_2]}{dt} = 1.05*10^{10}*[CO]*[O_2]^{0.5}*[H_2O]^{0.25}*MW_{CO_2}*e^{\left(\frac{-14293}{T}\right)} \quad [10]$$

$$\Re_3 = \frac{-10174.876*(1-\varepsilon)}{d*\varepsilon}\left(T*e^{\left(\frac{-50000}{1.97*T}\right)}\right)\left(\rho_{mix}*y_{CO_2}\right) \quad [11]$$

Where: ε is the porosity factor ($\varepsilon = 0.9$ for typical coal). $\rho_{O_2,\infty}$ is the density of oxygen in the incoming stream (far from the coal). d is the char particle mean diameter. MW_C is the molecular weight of carbon. T is the temperature. Φ is the ventilation factor. D_{O_2-char} is the binary diffusion coefficient between char and oxygen. Re_d is the Reynolds number. Sc is the Schmidt number.$[CO_2]$, $[CO]$, $[O_2]$, $[H_2O]$ are the concentrations of carbon dioxide, carbon monoxide, oxygen, and water vapor respectively. MW_{CO_2} is the molecular weight of carbon dioxide.

From the above rate expressions, it is possible to obtain the rates of species production. Thus:

$$\dot{w}_C = \Re_1 \text{ …….....}/\text{unit gas volume.}$$

$$\dot{w}_{CO_2} = \frac{\Re_3}{2} - \Re_2 \text{ ……}/\text{unit gas volume.}$$

$$\dot{w}_{CO} = \Re_2 - \Re_1 - \Re_3 \text{ …..../unit gas volume.}$$

$$\dot{w}_{O_2} = \frac{\Re_1 + \Re_2}{2} \text{ ……}/\text{unit gas volume.}$$

The above semi global model is considered simple in the sense that it does not involve any elementary reactions of chemical adsorption (surface complexes formation and combination). This model will be implemented in this work as a starting point in chemical modeling. More developed surface complex models may be evaluated for better results

4. Numerical Solution

The conservation laws (mass and energy) will be applied and numerically solved on each grid section. The numerical solution will provide the temperature and species concentrations (CO, among others) in each of the charcoal sections during each differential time step. We are specifically interested in the CO mass flow rate exiting the bottom charcoal slice. The total CO mass yielded over the entire smoking session is then computed by summing (over the total time of the smoking session) this CO mass flow rate (for the bottom section) multiplied by the time step. By varying the puff intervals and the interpuff duration, it is possible to simulate periodic or stochastic smoking schemes.

In obtaining the numerical solution, it is assumed that the species conservation equations are quasi-steady. Owing to the relatively low density of the gaseous phase, it may be assumed that the source terms and the convective terms dominate the accumulation terms in the species conservation equations. In other words,

$$\frac{\partial(\rho_{mix}Y_i)}{\partial t} << \frac{d}{dx}(\dot{m}_i'') \text{ and } \frac{\partial(\rho_{mix}Y_i)}{\partial t} << MW_i * \dot{w}_i$$

Thus, the accumulation terms may be neglected in the species conservation equations. This is the widely known assumption of a pseudo transient model established by Thorsness et al., 1978 [65].

After taking above simplifying assumption, equations 1 through 5 become:

$$\frac{d}{dx}(\dot{m}''_{H_2O}) = MW_{H_2O} * \dot{w}_{H_2O}$$

$$\frac{d}{dx}(\dot{m}''_{CO_2}) = MW_{CO_2} * \dot{w}_{CO_2}$$

$$\frac{d}{dx}(\dot{m}''_{CO}) = MW_{CO} * \dot{w}_{CO}$$

$$\frac{d}{dx}(\dot{m}''_{O_2}) = MW_{O_2} * \dot{w}_{O_2}$$

$$(\rho_{bed}C_{bed})\frac{dT}{dt} = \left(\dot{m}''_{mix}\varepsilon C_P \frac{dT}{dx}\right) + \left(\left[k_{gas}(\varepsilon) + k_{Solid}(1-\varepsilon)\right]\frac{d^2T}{dx^2}\right) + \left(\sum h^o_{f,i}\dot{w}_i\right)$$

Where at each time step, the energy equation is solved using the MATLAB pde solver (pdepe, [66]) to get the temperature profile. This profile is then used as an initial condition to calculate the reaction rates throughout the bed and then solve the steady state chemistry equations using the newly calculated rates. Thus, the temperature solution defines the new time step. When the energy equation is solved, a new time step begins. In

this new time step, the species conservation ordinary differential equations are solved to obtain the species profiles at this new time step.

C. Experiments Description

As previously mentioned, this thesis is aimed at studying the phenomenon of carbon monoxide production in the burning charcoal of a narghile waterpipe. For this purpose, experimental measurements will be performed. These measurements will directly address the research question posed in Chapter I, and will also serve to provide a standard against which the computational model will be validated. Thus, charcoal samples will be burned on the head of a real narghile to measure the average concentration of carbon monoxide produced in a real (stochastic) smoking session versus an equivalent periodic smoking session. Figure 3.5 shows a schematic of the experimental setup that will be implemented in order to accomplishing the above proposed experimental scheme.

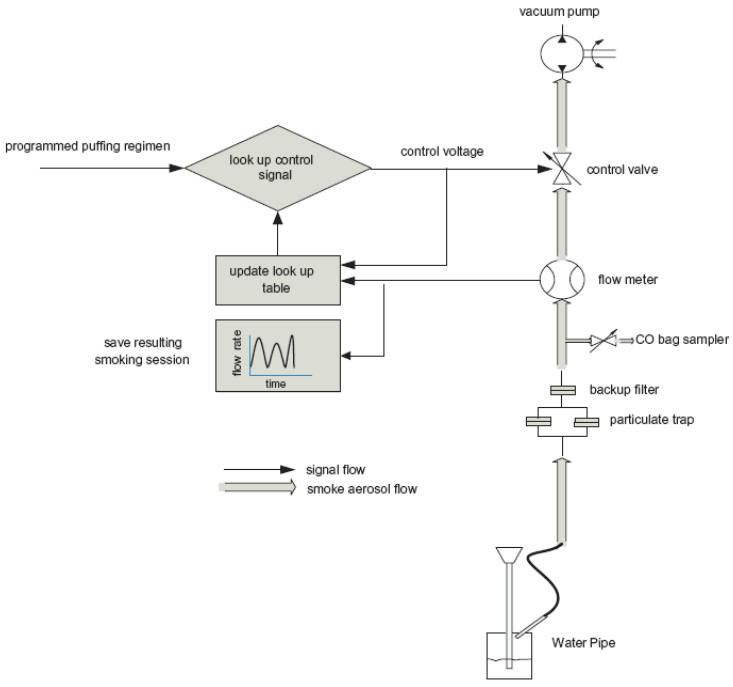

Fig 3.4: Schematic of the digital smoking machine used to produce smoking sessions.

Source: [12]

The experimental setup used in this work is the smoking machine that was already built and operated in the Aerosol Laboratory in AUB.The following explanation for the smoking machine is taken from Shihadeh et al. [12].

> "The smoking machine relies on a high-flow vacuum pump which is modulated by an electronic proportional control valve. The programmable inputs to the smoking machine include puff duration, flow rate, interpuff interval, and total number of puffs. The control valve signal is generated using feedback control provided by a PC-based data acquisition and control (DAQ) system. The feedback is provided by an electronic mass flow meter whose output signal is constantly sampled and recorded in a look up table containing valve control voltages and the resulting flow rates. Prior to the first smoking session, a calibration program is run which increments the valve control voltage signal from zero to the maximum value, thus initializing the lookup table. Once a smoking session is started, the initial values in the table are dynamically updated as flow conditions change (e.g., as pressure drop across filters increases, or as filters are replaced)."

CHAPTER 4

EXPERIMENTAL RESULTS

The experimental setup described previously has been used to play back several of the real life smoking sessions gathered by Shihadeh et al. [2] during a field study in 2002 till 2003 conducted in a café in Beirut, Lebanon. In this study, 52 volunteer smokers (14 females and 38 males) with a median age of 21 years have had a portable smoking topography instrument attached to their waterpipes prior to commencement of smoking. The volunteers have been then left to smoke at their own free pace. Thus, the real, unattended smoking topographies for these 52 smokers have been recorded.

Forty-five of these real life smoking sessions have been randomly chosen from the 52 sessions recorded in the study previously mentioned. The experimental setup described in the previous chapter has been used to play back these 45 smoking sessions. The CO yield for each of these sessions has been measured and recorded. On the other hand, the equivalent steady periodic sessions of the above real life smoking sessions have also been experimentally played back. Once again, the CO produced in these sessions has been also recorded. A basic experimental comparison has been thus established. The CO yield of each of the 45 real smoking sessions has been compared with the CO yield of its equivalent steady periodic session. Only 30 minutes of the original real smoking sessions have been reproduced. For each smoking session only one cylindrical charcoal (R=1.8 cm, L=1cm) has been used (brand: Three Kings, Holland made).

It has been determined by Monzer and Shihadeh [16] that most of the CO inhaled by narghile smokers originates from the charcoal smoldering and not from the tobacco. Therefore, the tobacco of the narghile used in this experimental setup has been removed. On the other hand, the hose and the water content of the narghile bowl were removed to factor out air infiltration through the nozzle and any CO dissolving in water. On the other hand, the tobacco of the narghile head has also been removed since most of the CO produced in a narghile comes from the charcoal and not the tobacco [16].

A. CO Yield Difference

After running the smoking sessions experimentally, and after verifying the validity of the obtained data, the data is analyzed and compared. Figure 4.1 shows a plot of the CO mass yield from the real smoking sessions versus the CO mass yield from their equivalent steady periodic sessions. From the experimental results shown in Figure 4.1, it is concluded that real smoking sessions yield more CO than their equivalent steady periodic sessions. The experiments performed have determined that real smoking sessions yield on average 16% more CO (mass) than their equivalent steady periodic sessions. This implies that a real smoker usually inhales about 16% more CO than that predicted by the standard methods of smoking experimentation that replace a real smoking profile with its equivalent steady periodic representation.

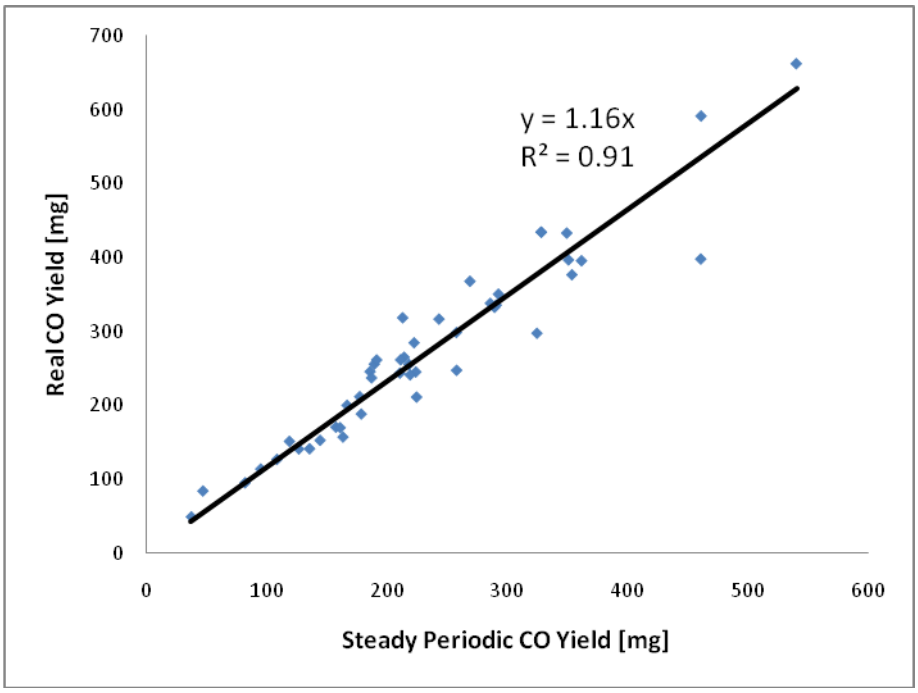

Fig 4.1: Experimental real smoking sessions CO yield versus steady periodic yield. The real sessions correspond to 45 human subjects recorded in Beirut area cafés.

B. Validity of Compared Data: Student's T-test

To verify the validity of the obtained results, the widely used Student's T-test is implemented to the compared values. The paired T-test is applied to the two populations in hand (where one population contains the real smoking sessions and the second population contains the equivalent steady periodic sessions). The T-test determines the probability of the null hypothesis that the two groups do not differ. In the current study, the test determines whether the groups (real and periodic sessions) have a statistically significantly different mean or whether with the measured difference in mean occurs by chance. The test gives a probability of less than $1.8*10^{-8}$% for the experimental populations (CO mass yield) to have occurred by chance. This test verifies the validity of all the experimental data to a significance level of almost 100%.

C. Reasons for CO Yield Trend

The reasons for the greater CO yield in real smoking sessions are investigated. In Table 4.1 several smoking topography parameters are cross checked with the CO yield of experimental playbacks to determine whether a statistically significant correlation exits among them. In this study, two parameters are considered to be correlated based on the Pearson's correlation coefficient (R^2) for a two tailed test (which determines the statistical significance of a correlation between 2 parameters). If the statistical significance level is 95% or more, a correlation is assumed to exist.

Table 4.1: Correlations among smoking topography parameters and the experimental CO concentration yield. The shown correlations are obtained by experimental playbacks of 45 human subjects recorded in Beirut area cafés. A correlation is said to exist if the Pearson's correlation coefficient (R^2) for a two tailed test yields a significance level is 95% or more.

	[CO] of Real Smoking Session	[CO] of Periodic Smoking Session
Average Flow Rate	✓	✓
Average Puff Duration	x	x
Average Interpuff Interval (IPI)	x	x
Smoke Volume	x	x
Number of Puffs	x	x
Filtered Average IPI	x	x
Stdev of IPI	x	x
Stdev of Puff Average Flow Rate	x	x
Stdev of Puff Duration	weak	x
Stdev of Puff Volume	x	x
Stdev of Filtered IPI	x	x

It should be noted that the filtered IPI means the interpuff interval of a filtered smoking session. In a filtered smoking session, all interpuff interval longer than 3 standard deviations are removed from the session.

Therefore, drawing from the results shown in Table 4.1, it is noticed that the only correlation shows between CO yield and flow rate. Two plots of CO concentration yield versus flow rate have been obtained for both real smoking sessions and their equivalent steady periodic session (Figure 4.2 and Figure 4.3). From these plots, it can be observed that CO yield is negatively correlated with flow rate (the greater the flow rate through the charcoal, the lower the CO concentration yield, for both real and steady periodic sessions).

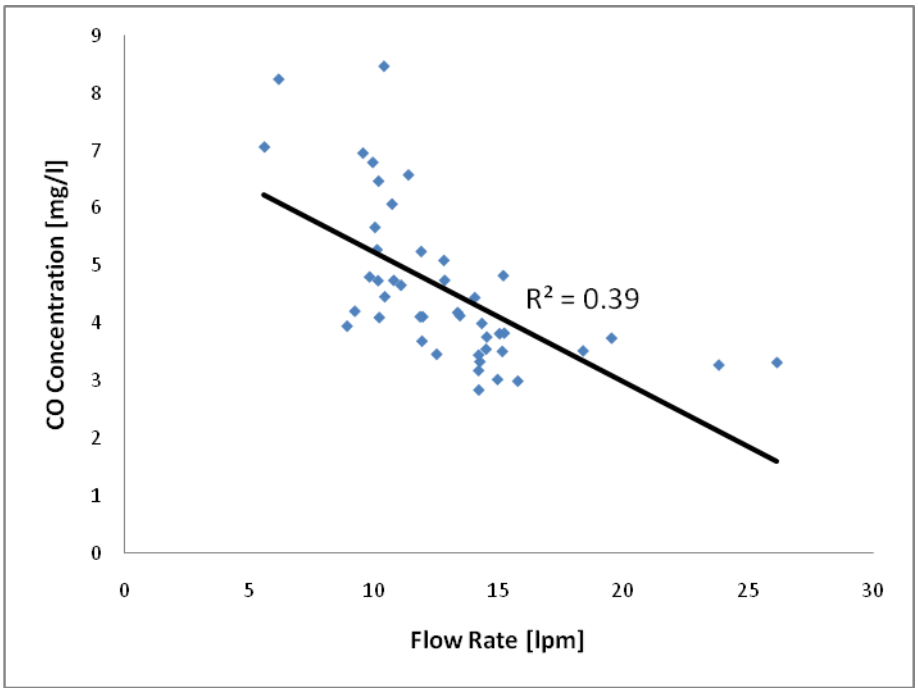

Fig 4.2: Experimental real smoking sessions CO yield versus smoking sessions average flow rate. The real sessions correspond to 45 human subjects recorded in Beirut area cafés.

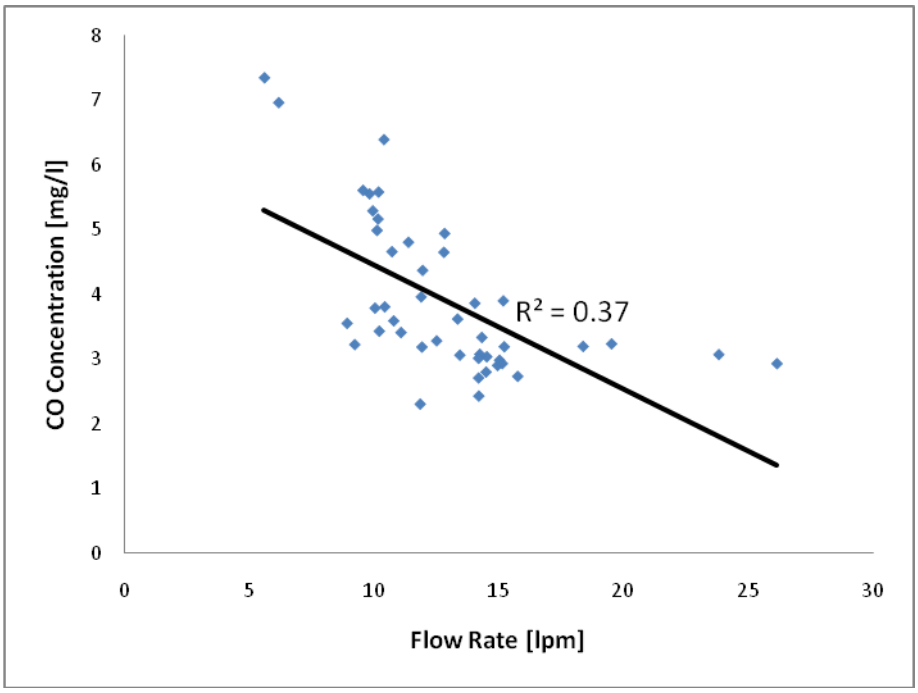

Fig 4.3: Experimental steady periodic sessions CO yield versus smoking sessions average flow rate. The steady periodic sessions are the equivalent of the real sessions corresponding to 45 human subjects recorded in Beirut area cafés.

D. Analysis and Conclusions

The experiments described in this chapter show that real smoking sessions yield on average 16% more CO than their equivalent steady periodic sessions. It is also shown that the only statistically significant correlation of any puffing paremeter is observed between CO yield and flow rate. The greater the average flow rate of a smoking session, the lower the CO concentration yield of that smoking session. These observations raise several questions. Why do real smoking sessions yield more CO mass than their equal volume steady periodic ones? Since CO yield increases with decreasing flow rate, does the averaging of low flow rates in steady periodic smoking sessions cause the discarding of major amounts of CO yield? What is the main reason that causes the flow rate to have such an effect on the CO produced from a smoking session? Is the temperature profile inside the

charcoal bed the key factor? Or, is it that the availability and the chemical interactions of various species drastically influence the CO yield? What are the physical phenomenon that could explain the behavior of the charcoal and the observed trends between flow rate and CO yield? To answer the previous questions, the numerical simulation code has been employed to understand how physical phenomenon such as temperature, species, and chemical kinetics interact together to produce these observed trends.

CHAPTER 5

NUMERICAL MODEL PERFORMANCE COMPARED TO EXPERIMENTS

The experiments performed in this work have shown that real smoking sessions produce 16% more CO than their equivalent steady periodic sessions. In addition, it has been determined that the greater the average flow rate of a smoking session, the lower its CO concentration yield will be, and that no other investigated parameter correlates with CO yield. However, these experimental results do not reveal the reasons that cause the CO production trends to be as such. Therefore, the numerical model outlined in Chapter 3 is utilized in an attempt to elucidate the physical phenomena underlying CO production trends and to explain the experimental results shown in Chapter 4.

Thirty-eight real smoking sessions and their equivalent steady periodic sessions have been simulated using the numerical code. The results obtained from these smoking sessions have been compared with the experimental results obtained for the same sessions. This comparison is essential to establish whether the numerical model and experimental results agree. Since the numerical model is intended to explain the reasons of the trends that appear in the experiments, it is therefore crucial to verify that the numerical simulation model agrees with the experiments in terms of showing these basic trends.

A. CO Yield Difference

After running the smoking sessions using the numerical simulation code, and after verifying the validity of the obtained data, the data is analyzed and compared. The

numerical simulations performed have determined that real smoking sessions yield on average 23% more CO (mass) than their equivalent steady periodic sessions. The experiments have showed this increase to be 16%. Therefore, the numerical model agrees with the experiments that real smoking sessions yield on average about 20% more CO than their equivalent steady periodic sessions. Figure 5.1 and Figure 5.2 show the increased CO yield in real smoking sessions for both the numerical simulations performed in this work.

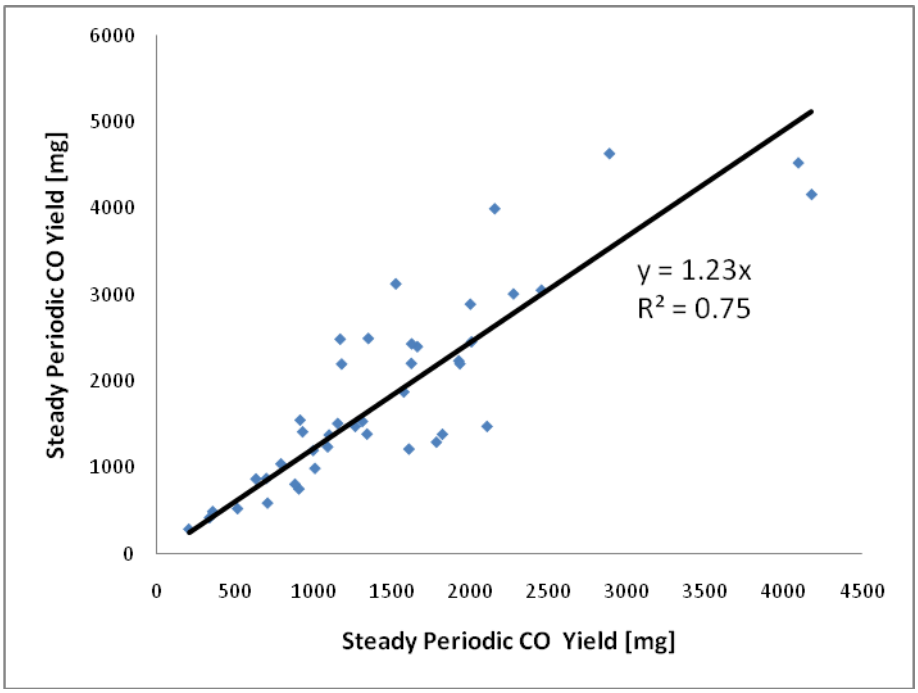

Fig 5.1: Numerical simulations real smoking sessions CO yield versus steady periodic yield. The real sessions correspond to 38 of the 45 human subjects recorded in Beirut area cafés.

B. Validity of Compared Data: Student's T-test

To verify the validity of the results obtained from the numerical simulation code, the widely used Student's T-test is again implemented to the compared values. The paired T-test is applied to the two populations in hand (where one population contains the real

smoking sessions and the second population contains the equivalent steady periodic sessions). The test gives a probability of less than 10^{-4}% for the numerical simulations populations (CO mass yield) to have occurred by chance. For experiments, the T-test gave $1.8*10^{-8}$% for the experimental populations (CO mass yield) to have occurred by chance .This test verifies the validity of all the data obtained by both experiments and simulations to a significance level of almost 100%.

C. Reasons for CO Yield Trend

Having established that the numerical simulation model agrees with the experiments in terms of showing a greater CO yield for real smoking sessions, the reasons for the increased CO yield in real smoking sessions are investigated and checked for agreement with the experimental results. Once again, several smoking topography parameters are cross checked with the numerical model CO yield in an attempt to seek correlations between such parameters and the yielded CO concentration of the smoking sessions. In this study, two parameters are considered to be correlated based on the Pearson's correlation coefficient (R^2) for a two tailed test (which determines the statistical significance of a correlation between 2 parameters). If the statistical significance level is 95% or more, a correlation is assumed to exist.

Table 5.1 shows whether a certain parameter is correlated with the other or not for both experimental and numerical simulations.

Table 5.1: Comparison of correlation detection between the numerical simulation code and the experimental palybacks. The shown experimental correlations correspond to 45 human subjects recorded in Beirut area cafés. The numerical simulation correlations correspond to 38 of the 45 human subjects. A correlation is said to exist if the Pearson's correlation coefficient (R^2) for a two tailed test yields a significance level is 95% or more.

	Experiments		Simulation	
	[CO] of Real Smoking Session	[CO] of Periodic Smoking Session	[CO] of Real Smoking Session	[CO] of Periodic Smoking Session
Average Flow Rate	✓	✓	✓	✓
Average Puff Duration	x	x	x	x
Average Interpuff Interval (IPI)	x	x	x	x
Smoke Volume	x	x	x	x
Number of Puffs	x	x	x	x
Filtered Average IPI	x	x	x	x
Stdev of IPI	x	x	x	x
Stdev of Puff Average Flow Rate	x	x	x	x
Stdev of Puff Duration	weak	x	✓	✓
Stdev of Puff Volume	x	x	x	x
Stdev of Filtered IPI	x	x	x	x

In agreement with the experimental data, it is established the strongest correlation shows between CO concentration yield and flow rate. Table 5.1 shows that the numerical model is able to predict that a relation exists between the flow rate and the CO yield (for both the real smoking sessions and the steady periodic ones).

Once again, from Fig 5.2 and Fig 5.3 it has been observed that CO yield is negatively correlated with flow rate (the greater the flow rate through the charcoal, the lower the CO concentration yield (for real and steady periodic sessions)). This same trend has been observed in the experimental results.

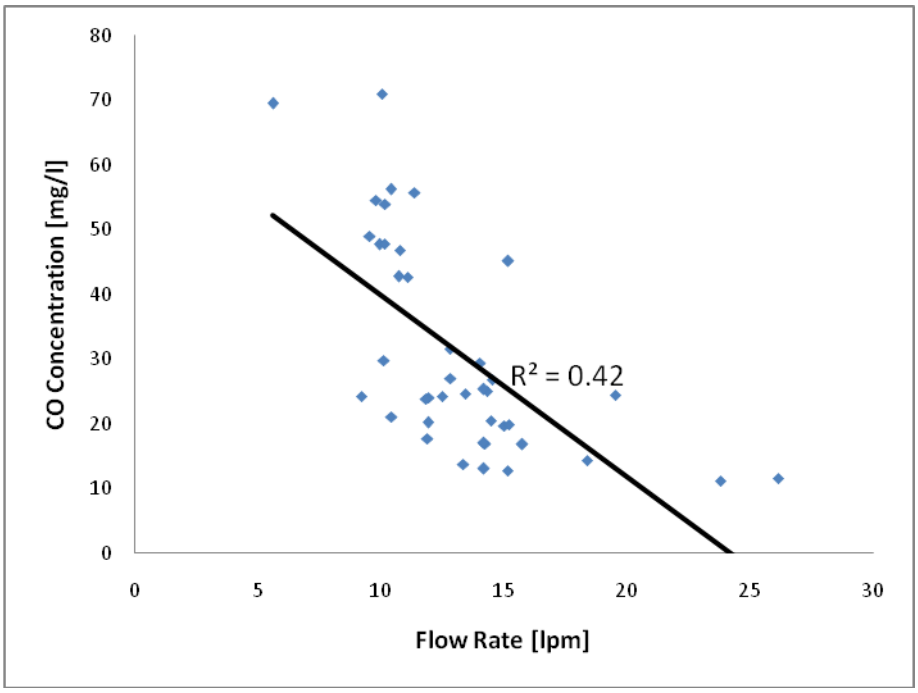

Fig 5.2: Numerical simulations real smoking sessions CO yield versus smoking sessions average flow rate. The real sessions correspond to 38 of the 45 human subjects recorded in Beirut area cafés.

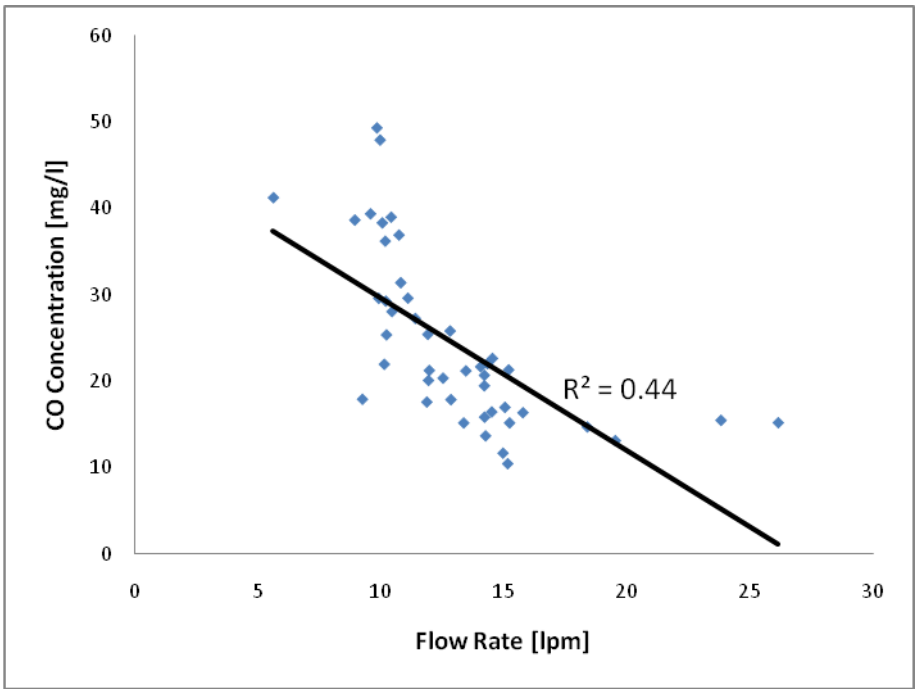

Fig 5.3: Numerical simulation steady periodic sessions CO yield versus smoking sessions average flow rate. The steady periodic sessions are the equivalent of the real sessions corresponding to 38 of the 45 human subjects recorded in Beirut area cafés.

D. Analysis and Conclusions

The experiments results presented in Chapter 4 show that real smoking sessions yield on average 16% more CO than their equivalent steady periodic sessions. The numerical model also shows that real smoking sessions yield on average 23% more CO than their equivalent steady periodic sessions. On the other hand, the experimental work shows that CO yield is negatively correlated with flow rate (greater flow rates produce less CO). The numerical simulations also show this trend. Thus, it is observed that the numerical simulation model is capable of producing the same trends observed in experimentation. Therefore, the numerical model valid for the purposes of this study.

CHAPTER 6

PHYSICAL PHENOMENA UNDERLYING CO PRODUCTION TRENDS

Experiments and computer simulations both showed that real smoking sessions produce more CO than their steady periodic equivalents. It has also been established that CO yield is negatively correlated with flow rate. To obtain a deeper understanding of the physical phenomena that cause such trends, the numerical model described in Chapter 3 has been used. Namely, it is sought to understand why do real smoking sessions yield more CO than their equivalent steady periodic sessions and why does the CO yield increase with lower flow rates.

From the previous analysis, it may be argued that the higher the flow rate of air through a charcoal bed, the lower the CO concentration yield will be. On the other hand, real life smoking sessions are characterized by a wide variability in flow rate. However, is it that the existence of a wide range of flow rates within a real smoking sessions and the fact that steady periodic smoking sessions ignore this wide variation in favor for one constant flow rate the main reason for the greater CO yield for real smoking sessions? To investigate this hypothesis, two controlled smoking sessions have been run experimentally and using numerical simulations. These smoking sessions all have 78 puffs, 3 second puff duration, 15 second interpuff interval, but varying flow rates and puffs of:

- Constant flow rate of 12.2 lpm.
- Alternating flow rate between 18.2 and 6.2 lpm (1 puff of 18.2 lpm followed by 1 puff of 6.2 lpm).

The rationale behind these two sessions is to evaluate the effect of flow rate variability. The first sessions does not contain any variability whereas the second session contains variability in flow rate only. It has been found that the alternating flow rate session yields on average 17.7 % more CO (concentration) than the constant flow rate session (the standard deviation of this increase was 7.2%). This result is obtained by experimentally running the above sessions three times. The paired two tailed T-test performed on the CO mass yield of each of the above sessions for the three experimental results showed that the data is more than 90% statistically significant.

The increased CO yield of the alternating flow rate session is observed although both sessions have the same average flow rate of 12.2 lpm and although everything else between the two sessions is the same, it is the flow rate variability that exclusively exits in the second session that caused the increase in the CO yield. This suggests that the lower flow rate existing within the alternating session (6.2 lpm for half the puffs) contributed to the production of more CO than what it did when averaged by the 18.2 lpm flow rate to have the same average flow rate of the alternating session, 12.2 lpm. In other words, the existence of the 6.2 lpm puffs within a session containing 18.2 lpm flow rate puffs, produces disproportionately more CO when compared to the 18.2 lpm puffs. More CO is yielded from the 6.2 lpm puffs to overcompensate for the lower CO yielded from the 18.2 lpm puffs. This means that whenever a smoking session contains puffs that have a variety of flow rates (like real life smoking sessions), the puffs having a flow rate lower than the average flow rate, produce more CO to overwhelm the low CO produced from puffs that have a flow rate greater than the average flow rate. This is exactly what smoking tests miss when the normally varying flow rates (between high and low) are replaced in favor for a

single average flow rate. This is the reason that makes real life smoking sessions yield about 16% more CO on average.

The reasons that cause the flow rate to have such an effect on CO yield are then investigated. Smoking sessions with constant flow rates of 6, 10, 12.2, 15, and 20 lpm are simulated using the numerical simulation code. From these simulations, plots of temperature, CO concentration, O_2 concentration, and CO_2 concentration versus bed depth are produced to study the effect of varying flow rate on the bed. Figure 6.1, Figure 6.2, Figure 6.3, and Figure 6.4 show these. These figures show the temperature and species profiles at the end of the 10^{th} puff of a smoking session that has a 3 second puff duration and a 15 second interpuff interval. On the other hand, a plot of the average of $e^{(-9465/T)}$ within the charcoal bed has been also produced for a smoking sessions of 3 second puff duration and 15 second interpuff interval but with flow rates of 6.2 lpm, 12.2 lpm, 18.2 lpm, and the case where the flow rate is alternating (changing between 6.2 lpm and 18.2lpm every puff). Figure 6.5 shows this plot. The plot shows two 3 second puffs followed by 15 sec interpuff intervals. The first puff is the 21^{st} puff of a steady periodic smoking session.

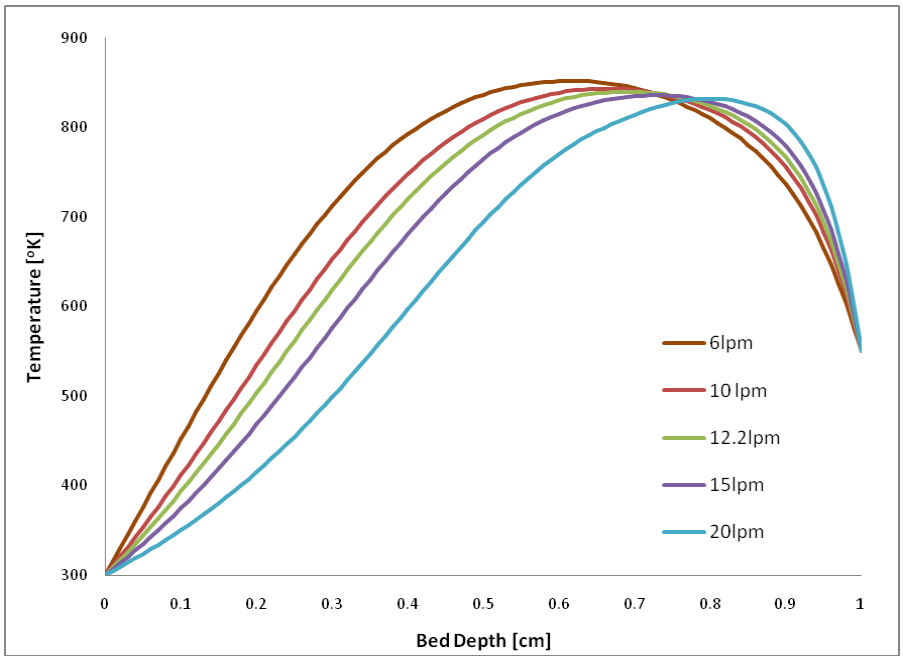

Fig 6.1: Temperature profiles versus bed depth for various flow rates. The plots are a snap shot of the temperature inside the charcoal bed at the end of the 10th puff of a steady periodic smoking session that has a 3 second puff duration and a 15 second interpuff interval.

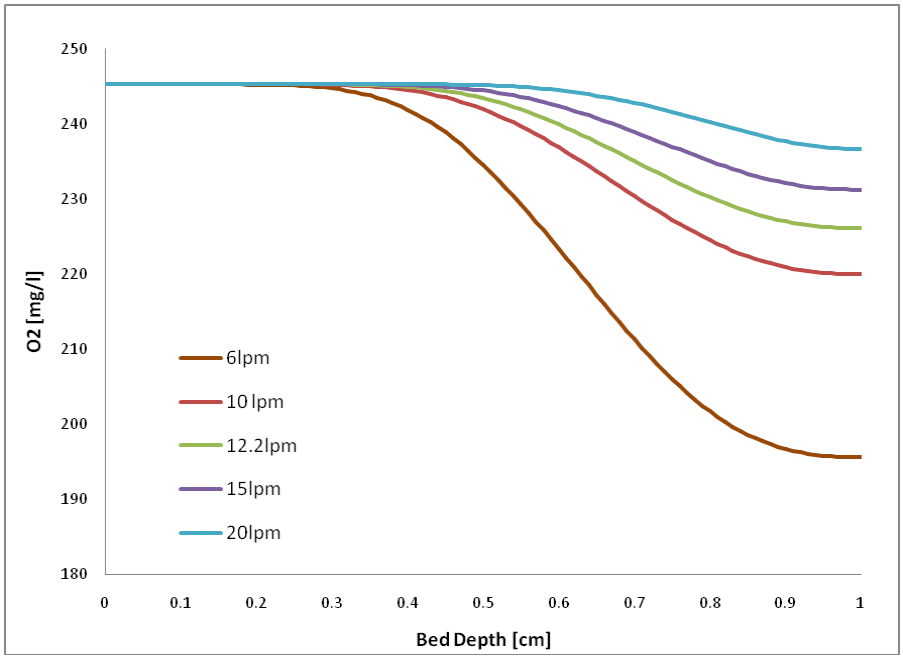

Fig 6.2: Oxygen profiles versus bed depth for various flow rates. The plots are a snap shot of the oxygen distribution inside the charcoal bed at the end of the 10th puff of a steady periodic smoking session that has a 3 second puff duration and a 15 second interpuff interval.

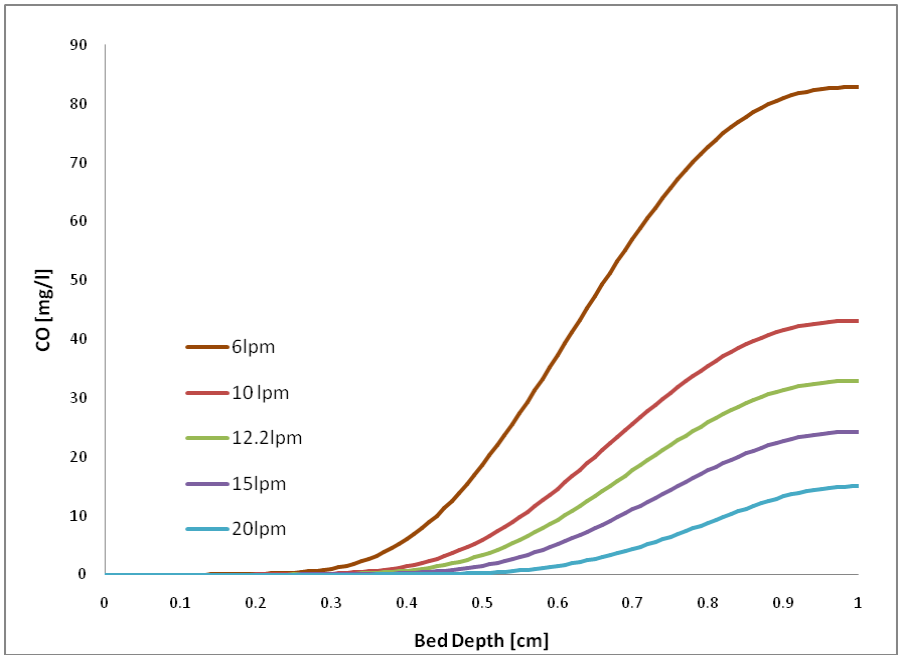

Fig 6.3: CO profiles versus bed depth for various flow rates. The plots are a snap shot of the CO distribution inside the charcoal bed at the end of the 10th puff of a steady periodic smoking session that has a 3 second puff duration and a 15 second interpuff interval.

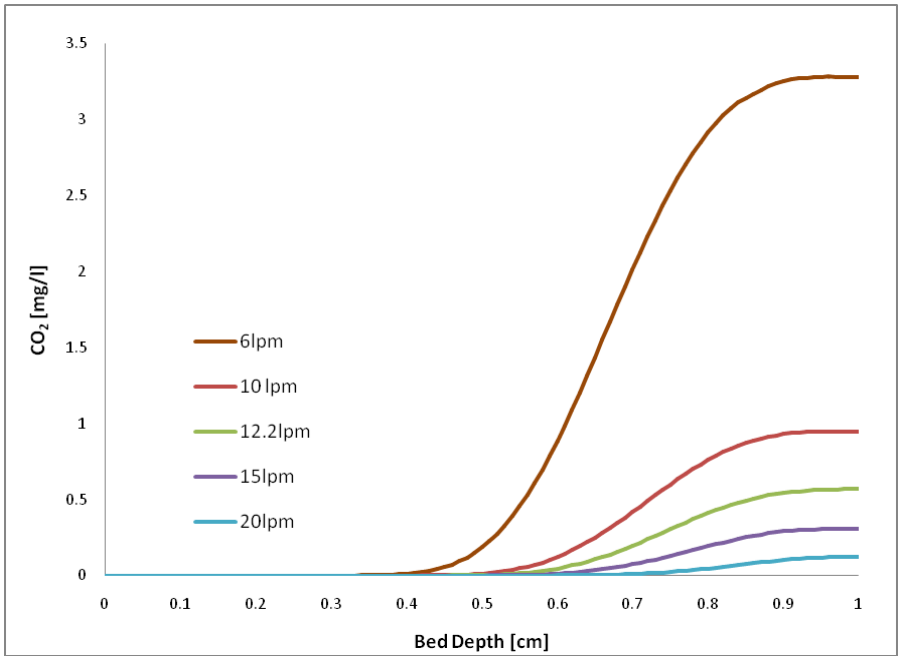

Fig 6.4: CO_2 profiles versus bed depth for various flow rates. The plots are a snap shot of the CO_2 distribution inside the charcoal bed at the end of the 10th puff of a steady periodic smoking session that has a 3 second puff duration and a 15 second interpuff interval.

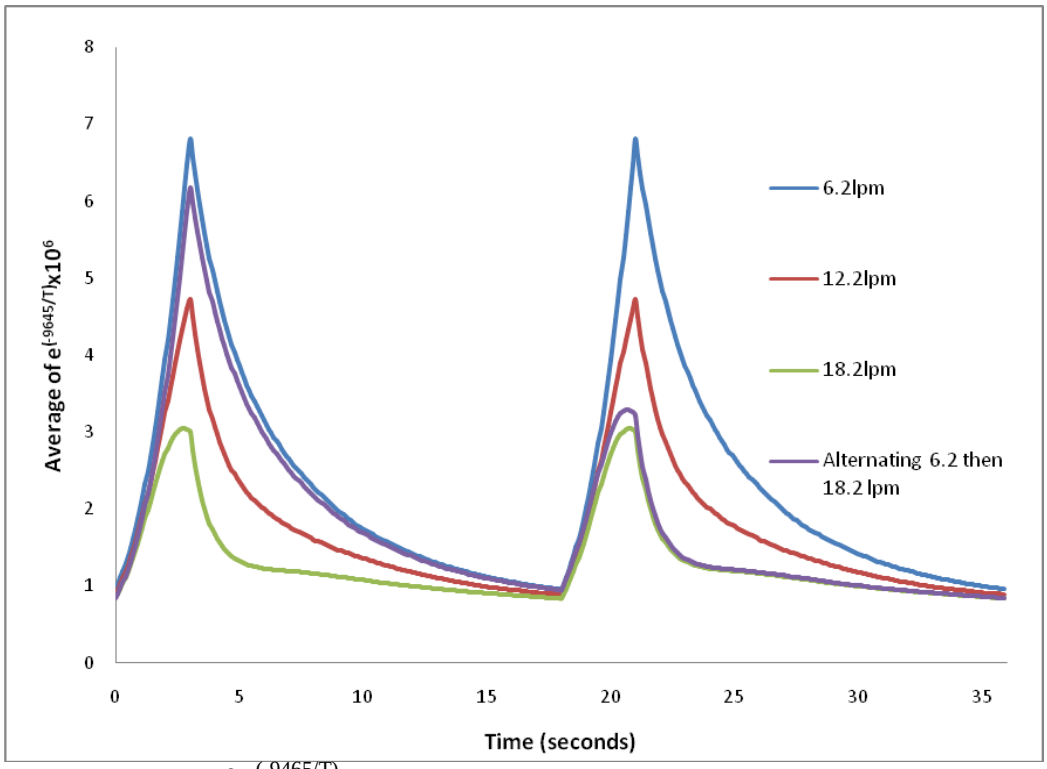

Fig 6.5: The average of $e^{(-9465/T)}$ inside the charcoal bed versus time. The plot shows two 3 second puff followed by 15 sec interpuff intervals. The first puff is the 21st puff of a steady periodic smoking session.

Figure 6.3 demonstrates that flow rates less than the average flow rate produce disproportionately more CO than flow rates that are equally greater than the average flow rate. It must be noted here that the CO inhaled by a smoker is the CO concentration exiting the bed. For example, a flow rate of 10 lpm is nearly the average flow rate of 6 lpm and 15 lpm. It is noticed that the CO yield of the average flow rate (10 lpm) is clearly not the average of the CO yield of the other two flow rates. There is a clear bias for the lower flow rate to produced more CO. The same analysis applies to the flow rates of 20 lpm and 10 lpm and their average flow rate of 15 lpm. This proves the fact that in real life smoking

sessions, the flow rates lower than the average produce disproportionately more CO than the flow rates that are equally greater than the average flow rate.

Figure 6.4 shows that oxygen is abundantly available within the charcoal bed and therefore the smoldering process is never oxygen limited. This means that when the flow rate is increased, more convective heat is lost to the air flow and this heat lost is not compensated by an increase in heat production by the exothermic chemical reactions because the increase in oxygen with increased flow rate simply passes through the bed without any effect (since the bed is already rich in oxygen at low flow rates). Therefore, higher flow rates through the charcoal bed cause an increase in convective heat loss without a corresponding increase in heat release, causing the temperature within the bed to drop.

Figure 6.1 and Figure 6.5 show that the peak temperature within the bed decreases as the flow rate through the bed increases. This explains the mechanism through which flow rate affect CO production in the charcoal bed. The greater the flow rate, the greater the convective heat loss from the char bed and thus the temperature in the bed is decreased (as seen in Figure 6.1). This temperature decrease consequently decreases the chemical rate by which CO is formed in the bed (the main chemical reaction producing CO in the bed is $C + \frac{1}{2}O_2 \rightarrow CO$ with a reaction rate in which the most contributing term is $e^{(-9465/T)}$ as seen in the expression of $\Re_1$). This may be observed in Figure 6.5 which shows that the greater the flow rate, the less would $e^{(-9465/T)}$ be, and this causes a direct decrease in CO yield.

From the previous discussion, it may be suspected that temperature is the key factor that dictates CO formation in the char bed. Nevertheless, a final test has been

conducted to prove whether the temperature or the characteristics of the flow is the dominant reason that explains why CO yield decreases with increased flow rate.

For the purpose of answering the pre-mentioned query, four numerical simulations have been performed. In first two of these simulations, the temperature profile of a 6 lpm puff is first established in the charcoal bed and then flow rates of 15 lpm and then 6 lpm are made to flow through the charcoal bed. In the second two of the four simulations, temperature profile of a 15 lpm is established in the charcoal bed and then flow rates of 15 lpm and then 6 lpm are made to flow through the charcoal bed. The CO yield for a 0.1 second time interval is computed. Table 6.1 describes the above four numerical simulations.

Table 6.1: The CO mass yield for controlled simulations for two cases in which the temperature profile inside the charcoal bed is fixed while the flow rate varies (the first two cases) and for two other cases in which the flow rate is fixed while the temperature profile varies. The CO is the yield of a 0.1 sec time interval.

Temperature Profile of	**Flow Rate of**	**mCO [mg]**
15 LPM	15 LPM	0.566
15 LPM	6 LPM	0.602
6 LPM	6 LPM	0.876
6 LPM	15 LPM	0.886

It is noticed that when the temperature profile is kept constant and the flow rates are varied (cases 1 with 2, and cases 3 with 4), the CO yield is nearly unchanged. Nevertheless, when the flow rate is kept constant and the temperature profile is varied (cases 1 with 4, and cases 2 with 3), the CO yield is nearly 60% more for the cases that have the 6 lpm puff temperature profile (the higher temperature).

It is concluded that the temperature is the key factor leading to the decreased CO yield with increasing flow rate. Varying the temperature at constant flow rate produces 60% more CO; whereas, varying the flow rate at constant temperature produces no difference in CO mass yield. This shows that temperature is the dominant factor behind the observed trend of increased CO yield with decreased flow rate. This relatively greater sensitivity to temperature is due to the fact that $\Re_1$ is exponential with temperature while being linear with the effects of flow rate, namely $[O_2]$.

It is concluded that the increased flow rate causes the peak temperature within the bed to drop because of the considerable increase in the convective heat loss (most of the flow is non reactive N_2). This temperature drop will significantly decrease the reaction rate by which CO is produced within the charcoal bed, $\Re_1$ (since the reaction rate is exponential in temperature). In fact, the temperature drop will also lower all the other chemical rates (because they too are exponential with temperature). Thus, the temperature drop leads to an overall decrease in chemical interactions within the bed. This decreased chemical action within the bed is translated to the observed decreased drop in the oxygen profile within the main reaction zone. It is also manifested in the decreased CO yield.

A. Final Conclusion

The greater the air flow rate through a smoldering bed of charcoal, the lower the CO yield. This is due to the fact that high levels of flow rate increased convective heat loss with the flow. This heat loss is greater than the increased heat production that may be caused by the existence of more oxygen with high flow rate. In other words, with greater air

flow rate, more oxygen will be available for combustion which should normally increase the temperature; however, this is counter acted by an increase in convective heat loss (this fact is demonstrated by the blow out phenomenon at very high flow rates) causing the observed temperature drop. This finding is further verified in the O_2 profiles within the charcoal bed in Figure 6.2 which shows that a smoldering charcoal bed on a narghile head is always oxygen rich (within the real life observed flow rates of smokers). This excess availability of oxygen causes an increased flow rate to increase the convective heat loss that is not compensated by chemical exothermic heat production. This causes the temperature of the charcoal bed to drop with increasing flow rates (since the increased flow simply passes through the bed without causing an increase in chemical heat production). This temperature drop in turn decreases the chemical rate by which CO is produced within the charcoal bed leading to the observation of less CO yield with increased flow rate.

It has been established that this temperature drop is the key factor leading to lower CO production inside the charcoal bed. This temperature drop decreases all the chemical rates within the bed (all chemical rates are exponential in temperature). This decrease in chemical rates leads to decreased chemical interactions and consequently less CO production.

Finally, it may be concluded that real smoking sessions produce more CO than their equivalent steady periodic ones. Flow rate seems to have a significant effect on the CO yield of smoking sessions. The lower the flow rate, the greater the CO yield. As shown before, the flow rate variability exiting in real life smoking sessions, or in other words, the existence of a range of different flow rates within real smoking sessions (and within a

single puff) contributes more CO than the case where these flow rates are masked by the constant average flow rate. Steady periodic representations of real life smoking sessions neglect all the flow rates that are lower or greater than the average flow rate (flow rate variations) within a smoking session for the favor of the average flow rate. Flow rates that are lower than the average flow rate produce disproportionately more CO than the flow rates that are equally greater than the average flow rate. This is what makes steady periodic sessions yield on average 16% less CO. The variation of the controlling parameters show that flow rate variability, and not variability in puff duration or interpuff interval, causes a real smoking session to exhibit higher CO yields than its steady periodic analog. Simulations indicate that this effect is derivative to slow chemistry relative to thermal convection in the relevant ventilation regime of this problem.

CHAPTER 7

SUMMARY AND FUTURE WORK

A. Summary

An investigation of CO yield in Narghile smoking was conducted. In particular, the concentration was on finding whether real stochastic smoking sessions yield the same CO as their equivalent steady periodic sessions. The study included experiments in which playbacks of real smoking sessions and their steady periodic equivalents were run on a smoking machine. The work also included a numerical simulation model to simulate the forward smoldering of the charcoal bed which is placed on the Narghile head and accounts for most of the CO produced in Narghile smoking (Shihade, Monzer, [16]). The data on CO yield of both the experiments and simulations was collected and it was determined that real smoking sessions produced more CO than their steady periodic equivalents. This increase was found to be 16% on average in experiments; and 23% on average in simulations. The reason for this trend was investigated. Many smoking profile parameters were cross checked for any correlations with CO yield (mainly CO concentrations). It was then determined that the key factor for CO yield difference was volume flow rate. It appeared that the more the flow rate through the charcoal, the less the concentration of the CO yield. This hypothesis was checked by experimentally running two controlled smoking sessions:

- 78 puffs, constant flow rate of 12.2 lpm
- 78 puffs, flow rate alternating between 18.2 and 6.2 lpm (changing with every puff)

It has been found that the alternating flow rate session yields on average 17.7 % more CO (concentration) than the constant flow rate session (the standard deviation of this increase was 7.2%). This showed that flow rate variability present in the alternating flow rate session (and not present in the constant flow rate session) contributed to the increased CO yield. This suggested that the lower flow rate in the alternating session (6.2 lpm for half the puffs) contributed to the production of more CO (more than what is produced when averaged by the 18.2 lpm session to give the same average flow rate of the alternating session, 12.2 lpm).

The attention was then shifted on finding the reason that causes flow rate to have such an effect on CO yield. The simulation code was mainly used for this purpose. Several smoking sessions with constant flow rates of 6, 10, 12.2, 15, and 20 lpm were simulated. Profile plots of temperature, CO concentration, O_2 concentration, and CO_2 concentration were produced. It was noticed that with greater flow rates, the temperature inside the charcoal was decreased. It was also noted that with greater flow rates, more O_2 exited the charcoal bed (the O_2 profile dropped considerably less in the reaction zone) leading to the existence of higher O_2 concentrations within the bed. The reason for such a temperature drop with high flow rates turned out to be that a smoldering charcoal bed on a narghile head is always oxygen rich (within the real life observed flow rates of smokers). This excess availability of oxygen causes an increased flow rate to increase the convective heat loss that is not compensated by chemical exothermic heat production. This causes the temperature of the charcoal bed to drop with increasing flow rates (since the increased flow simply passes through the bed without causing an increase in chemical heat production). This temperature

drop in turn decreases the chemical rate by which CO is produced within the charcoal bed leading to the observation of less CO yield with increased flow rate.

From the above observations, it may be concluded that temperature is the main reason that dictates CO production in a smoldering charcoal bed. Nevertheless, another test to prove the superiority of temperature over species availability has been performed. Four numerical simulations were conducted. In first two of these simulations, the temperature profile of a 6 lpm puff was first established in the charcoal bed and then flow rates of 15 lpm and then 6 lpm were made to flow through the charcoal bed. In the second two of the four simulations, temperature profile of a 15 lpm was established in the charcoal bed and then flow rates of 15 lpm and then 6 lpm were made to flow through the charcoal bed. It was noticed that when the temperature profile is kept constant and the flow rates are varied, the CO yield is nearly unchanged. Nevertheless, when the flow rate is kept constant and the temperature profile is varied, the CO yield is nearly 60% more for the cases that have the 6 lpm puff temperature profile (the higher temperature).

it is concluded that the temperature was the key factor leading to the decreased CO yield with increasing flow rate. Varying the temperature at constant flow rate (constant species availability while varying temperature) produces 60% more CO mass flux; whereas, varying the flow rate at constant temperature (constant temperature while varying species availability) produces no difference in CO mass flux. This shows that temperature is the dominant factor behind the observed trend of increased CO yield with decreased flow rate. This relatively greater sensitivity to temperature is due to the fact that $\Re_1$ is exponential with temperature while being linear with species (flow rate).

The final conclusion is that with increased flow rate, convective heat loss within the charcoal bed in considerably increased leading to a drop in the temperature profile within the bed. This temperature drop decreases the chemical kinetics of the chemical reactions occurring within the bed. This, in turn, causes less CO production with increased flow rate. Real smoking sessions have a wide variety of flow rates. A normal typical puff ramps up from a zero flow rate and then oscillates among a range of flow rates. On the other hand, a steady periodic smoking session does not capture the variability in flow rates existing in a real smoking session and keeps the flow rate at an average value which is considerably greater than the low flow rates observed within a real puff. It is these low flow rates that cause the CO yield in real smoking sessions to be greater than the yield of their equivalent steady periodic sessions. This is because flow rates lower than the average flow rate produce disproportionately more CO than flow rates that are equally greater than the average flow rate.

B. Future Work

The main aim of this work was to study the effect of representing a real Narghile smoking session by its equivalent steady periodic session. This was accomplished through experimentation and by a numerical simulation model. The simulation model was constructed and solved to provide an insight to the basic physical phenomena occurring within a smoldering bed of charcoal. The numerical model has succeeded in its ultimate purpose and captured the basic physical trends of CO yield. This said, it must be noted that the model still misses several aspects of the real life charcoal smoldering processes. This is manifested in the fact that the numerical code gives CO concentration values that are about

one order of magnitude greater than real life values (average proportional factor of 6.5). This could be caused by the absence of several real life aspects within the model. It is suggested that these aspects be incorporated in the future version of the model. Such future work should include

- Enhanced chemistry: The chemical mechanism producing CO in the current model is simplistic. Several advanced chemical models exist (some were described in the literature review chapter). The incorporation of such advanced chemical models (especially those with carbon-oxygen surface complexes) should provide for a better chemical 'description' of how different species interact within a charcoal bed to produce the various species found therein.

- Ash modeling: Ash formation is an important phenomenon that occurs whenever charcoal is smoldered. The existence of ash has profound effects on the temperature profile within the bed, as well as on the diffusion of air to and away from the reaction zone (availability of oxygen). The addition of an ash model would make modeling the smoldering process closer to real smoldering.

- Particle shrinkage and fuel depletion: In the current model, particles assume a constant shape and size, and thus the char bed is assumed to retain its size and mass throughout the smoldering process. This may be the main reason of the elevated CO yields observed in the numerical simulation code (when compared to experiments). In future models, it is suggested that a particle shrinkage sub-model be added alongside with equations that describe fuel depletion (a particle number depletion equation is mostly used for this purpose and it is described in the literature review chapter).

- Flow passage routes: In the current model, all the flow is assumed to pass directly through the bed. In real narghile setups, air passage is not that idealized. It is believed that a significant amount of air flow passes along the vertical periphery of the charcoal bed and directly mixes with the flow emerging out of the smoldering bed. This is believed to provide a significant diluting effect. This could also explain the lower CO yield observed in experiments (when compared to the simulation code). The air flow along the vertical periphery of the charcoal bed also affects the whole smoldering process. Such a peripheral flow could give rise to other reaction zones within the bed, or simply cause a shift in the position of the reaction zone, or both. Such aspects need to be addressed in future studies.

- Split energy equations: the current model assumes that the temperature of the solid phase and the gaseous phase are the same. This is mainly because of the assumption that the flow passage through the charcoal bed makes an intricate path through many pores. In reality, the temperature profiles of the gaseous and the solid phases are not the same. Incorporating an independent energy equation for each phase results in different gas and solid temperatures within the bed, and thus leads to a better model.

Finally, it could be argued that the current simulation model has captured the basic physical phenomena of charcoal smoldering and it has showed the reasons behind the CO yield trends described in this study. It is a first order model intended for this purpose, and it could be said that it has been sufficient to serve its purpose within the current study. Nevertheless, the smoldering process occurring in a char bed on a narghile head still possesses several real life phenomena that could be incorporated into the model. It is the

proper modeling of these phenomena that should constitute the backbone of future work performed to further expand and continue this work.

BIBLIOGRAPHY

1. Shihadeh, A.; Saleh, R. Polycyclic aromatic hydrocarbons, carbon monoxide, ‘‘tar’’, and nicotine in the mainstream smoke aerosol of the narghile water pipe. *Food and Chemical Toxicology.* **2005**, 43, 655–661.

2. Shihadeh, A.; Azar, S.; Antonios, C.; Haddad, A. Towards a topographical model of narghile water-pipe cafe´ smoking: a pilot study in a high socioeconomic status neighborhood of Beirut, Lebanon. *Pharmacology, Biochemistry and Behavior.* **2004**, 79, 75–82.

3. Cronje, F.; Carraway, M.; Freiberger, J.; Suliman, H.; Piantadosi, C. Carbon monoxide actuates O_2-Limited Heme Degradation in the rat brain. *Free Radical Biology and Medicine.* **2004**, 37, 1802–1812.

4. Patel, A.; Moody, J. Sneyd, R.; Handy, R. Carbon monoxide exposure in rat heart: evidence for two modes of toxicity. *Biochemical and Biophysical Research* Communications. **2004**, 321, 241–246.

5. Herman, L.; Carbon monoxide poisoning presenting as an isolated seizure. *Journal of Emergency Medicine*. **1998**, 16, 429–432**.**

6. Gorman, D.F.; Huang, Y.L.; Williams, C. Prolonged exposure to one percent carbon monoxide causes a leucoencephalopathy in un-anaesthetized sheep. *Toxicology*. **2001**, 165 97–107**.**

7. Borman, G.L. Combustion Engineering, McGraw Hill, New York, **1998**.

8. Harvey W.R.; Hutton, P. Carbon monoxide: Chemistry, role toxicity and treatment. *Current Anaesthesia & Critical Care*. 10, 158–163, **1999.**

9. Surgeon General's report. **2004.**

10. Hurt, R.H.; Calo, J.M. Semi-Global Intrinsic Kinetics for Char Combustion Modelling. *Combustion and Flame.* **2001**, 125, 1138–1149.

11. Antal, M.J.; Grønli, M. The Art, Science, and Technology of Charcoal Production. *Ind. Eng. Chem. Res.* **2003,** *42,* 1619-1640.

12. Bews, I.M.; Hayhurst, A.N.; Richardson, S.M.; Taylor, S.G. The Order, Arrhenius Parameters, and Mechanism of the Reaction Between Gaseous Oxygen and Solid Carbon. *Combustion and Flame.* **2001,** 124, 231–245.

13. Smith, I.W. The Combustion Rates of Coal Chars: A Riview. *Nineteenth Symposium (International) on Combustion; The Combustion Institute: Pittsburgh*, **1983,** pp 1045–1065.

14. Libby, P. A.; Blake, T. R. Combustion of a Spherical Carbon Particle in Slow Viscous Flow. *Combusion and Flame.* **1991,** 86, 147–161.

15. Ryan, J.S.; Hallett, W.H. Packed bed combustion of char particles: experiments and an ash model. *Chemical Engineering Science.* **2002,** 57, 3873–3882.

16. Hayhurst, A. N.; Parmar, M. S. Does solid carbon burn in oxygen to give the gaseous intermediate CO or produce CO_2 directly? Some experiments in a hot bed of sand fluidized by air. *Chemical Engineering Science.* **1998,** 53, 427–438.

17. Bedwani, R.; El-Khwsky, F.; Renganathan, E.; et al. Epidemiology of bladder cancer in Alexandria, Egypt: tobacco smoking. *Int J Cancer.* **1997,** *73,* 64–67.

18. Shihadeh, A. Investigation of mainstream smoke aerosol of the argileh water pipe. *Food and Chemical Toxicology.* **2003,** *41,* 143–152.

19. Attah, K.. Smoke the dull hours away through argilehs. *The Star, Emerging Markets Datafile. Jordan.* **28 August 1997**.

20. Shediac-Rizkallah, M.; Afifi Soweid, R.; Farhat, T.; Yeretzian, J.; Nuwayhid, I.; Sibai, A.; Kanj, M.; El-Kak, F.; Kassak, K.; Kanaan, N. Adolescent health-related behaviors in postwar Lebanon: findings among students at the American University of Beirut. *International Quarterly of Community Health Education.* **2002,** *20-2,* 115–131.

21. Knishkowy, B.; Amitai, Y. Water-Pipe (Narghile) Smoking: An Emerging Health Risk Behavior. *Pediatrics.* **2005,** *116,* 113-119.

22. Nafae, A; Misra, S.P.; Dhar, S.N.; Shah, S.N. Bronchogenic carcinoma in Kashmir Valley. *Indian J Chest Dis.* **1973,** *15,* 285–295.

23. Qiao, Y.L.; Taylor, P.R.; Yao, S.X.; et al. Relation of radon exposure and tobacco use to lung cancer among tin miners in Yunnan Province, China. *Am J Ind Med.***1989,** *16,* 511–521.

24. Gunaid, A.A.; Sumairi, A.A.; Shidrawi, R.G.; et al. Oesophageal and gastric carcinoma in the Republic of Yemen. *Br J Cancer.* **1995,** *71,* 409–410.

25. Larfeldta, J.; Lecknera, B.; Melaaen, C.M. Modelling and measurements of heat transfer in charcoal from pyrolysis of large wood particles. *Biomass and Bioenergy.* **2000,** 18, 507–514.

26. Kantorovich, I.I.; Bar-Ziv, E.; Heat transfer within highly porous chars: a review. *Fuel.* **1999,** 78, 279–299.

27. Kantorovich, I.I.; Bar-Ziv, E.; Role of porous structure in char oxidation. *Applied Thermal Engineering.* **1998,** 18, 991–1003.

28. Bhhattacharya, S.C.; Albina, D.O.; Abdul Salam, P. Emission factors of wood and charcoal-fired cookstoves. **2002.**

29. Monzer, B. Experimental investigation of the relative contributions of charcoal and tobacco to carbon monoxide and polycyclic aromatic hydrocarbon yields in the mainstream smoke of the narghile waterpipe. *Masters Thesis, American University of Beirut.* **2005.**

30. Hurt, R.H.; Haynes, B.S. On the origin of power-law kinetics in carbon oxidation *Proceedings of the Combustion Institute.* **2005,** 30, 2161–2168.

31. Li,C.; Brown, C.T. Carbon oxidation kinetics from evolved carbon oxide analysis during temperature-programmed oxidation. *Carbon.* **2001,** 39, 725–732.

32. Lear, A.E.; Brown, T.C.; Haynes, B.S. Oxygen Chemisorption on Carbon. *Twenty-Third Symposium (International) on Combustion, Orleans, France, Pittsburgh: The Combustion Institute*, **1991**, 1191–1198.

33. Gremyachkin, V.M.; Fortsch, D.; Schnell, U.; Hein, K.R.G. A Model of the Combustion of a Porous Carbon Particle in Oxygen. *Combustion and Flame.* **2002**, 130, 161–170.

34. Layrov, N.V.; Rosenfeld, E.I.; Khaustovich, G.N., *The Processes of Fuel Combustion and Protection of Environment.* Metallurgia, Moscow, **1981**.

35. Lee, S.; Angus, J.C.; Edwards, R.V.; Gardrer, N.C. *A.I.Ch.E. Journal.* **1981,** 30, 583.

36. Matsui, K. The Attachment of the Flame Sheet to the Carbon Surface in a Carbon Combustion Model: On the Combustion Rate. *Combustion and Flame.* **1999,** 118, 697–706.

37. Libby, P. A.; Blake, T. R. Theoretical Study of Burning Carbon Particles. *Combusion and Flame.* **1979,** 36, 139–169.

38. Matalon, M. Complete Burning and Extinction of a Carbon Particle in an Oxidizing Atmosphere. *Combustion and Flame.* **1980,** 24, 115–127.

39. Adomeit, G.; Hocks, W.; Henriksen, K. Combustion of a Carbon Surface in a Stagnation Point Flow Field. *Combustion and Flame.* **1985,** 59, 273–288.

40. Walker, P.L.; Taylor, R.L.; Ranish, J.M. An Update on the Carbon-Oxygen Reaction. *Carbon.* **1991,** 29, 411–421.

41. Marsh, H.; Kuo, K. Kinetics and Catalysis of Carbon Gasification. In: Marsh H, editor, Introduction to carbon science, London: Butterworths, **1989,** p.107.

42. Atamny F.; Blocker J.; Dubotzky A. *Molecular Physics.* **1992,** 76, 851.

43. Ahmed, S.; Back, M.H.; Roscoe, J.M.; A kinetic model for the low temperature oxidation of carbon. *Combustion and Flame.* **1987,** 70, 1–16.

44. Du, Z.; Sarofim, A.F.; Longwell, J.P.; Mims, C. Kinetic Measurement and Modeling of Carbon Oxidation. *Energy and Fuels.* **1991,** 5, 214–221.

45. Haynes, B. A Turnover Model for Carbon Reactivity I. Development. *Combustion and Flame.* **2001,** 126, 1421–1432.

46. Vastola, F.J.; Hart, P.J.; Walker, P.L.; A Study Carbon-Oxygen Surface Complexes using O^{18} as a Tracer. *Carbon.* **1964,** 2, 65–71.

47. Marsh, H.; Foord, A.D. *Carbon.* **1973,** 11, 421–424.

48. Lear, A.E.; Brown, T.C.; Haynes, B.S. Oxygen Chemisorption on Carbon. *Twenty-Third Symposium (International) on Combustion, Orleans, France, Pittsburgh: The Combustion Institute.* **1991**, 1191–1198.

49. Yang, W.; Ryu, C.; Choi, S.; Unsteady One-Dimensional Model for a bed Combustion of Solid Fuels. *Journal of Power and Energy.* **2004,** 218.

50. Hayhurst, A. N.; The Mass Transfer Coefficient for Oxygen Reacting with Carbon Particle in a Fluidized or Packed Bed. *Combustion and Flame.* **2000,** 121, 679–688.

51. Bhagat, M.P.; Wood Charcoal Combustion and the Effects of Water Application. *Combustion and Flame.* **1980,** 37, 275–291.

52. Thunman, H.; Leckner, B.; Co-current and counter-current fixed bed combustion of biofuel—a comparison. *Fuel.* **2003,** 82, 275–283.

53. Bruch, C.; Peters, B.; Nussbaumer, T. Modelling wood combustion under fixed bed conditions. *Fuel.* **2003,** 82, 729–738.

54. Leach, S.V.; Rein, G.; Ellzey, J.L.; Ezekoye, O.A. Kinetic and Fuel Property Effects on Forward Smoldering Combustion. *Combustion and Flame.* **2000,** 120, 346–358.

55. Cooper, J.; Hallett, W. L. H. A numerical model for packed-bed combustion of char particles. *Chemical Engineering Science.* **2000,** 55, 4451–4460.

56. Kittel C. Introduction to Solid State Physics. *Wiley.* New York. **1970.**

57. Guptaa, M.; Yanga, J.; Roy, C. Specific heat and thermal conductivity of softwood bark and softwood char particles. *Fuel.* **2003,** 82, 919–927.

58. Wakao, N.; Kaguei, S. Heat and Mass Transfer in Packed Beds. *Gordon and Breach.* New York. **1982.**

59. Adanez, J.; de Diego, F.L.; Garcia-Labiano, F.; Abad, A.; Abanades, C. J. Determination of Biomass Char Combustion Reactivities for FBC Applications by a Combined Method. *Ind. Eng. Chem. Res.* **2001,** 40, 4317–4323.

60. Cui, Y.; Stubington, F.J. A mathematical Model of in-bed Char Combustion of Australian Coals in PFBC. *Fuel.* **2001,** 80, 2049–2056.

61. Grønli, M. A Theoretical and Experimental Study of the Thermal Degradation of Biomass, *PhD Thesis. Division of Thermal Energy and Hydro Power, Trondheim.* **1996**.

62. Yagi, S.; Kunii, D. Studies on efective thermal conductivity in packed beds. *A.I.Ch.E. Journal.* **1957,** 3, 373–381.

63. Howard, J. B.; Williams, G. C.; Fine, D. H. Kinetics of carbon monoxide oxidation in postfame gases. *14th Symposium (International) on Combustion.* **1973,** pp. 975–986.

64. Laine, N.R.; Vastola, F.J.; Walker, P.L. *Journal of Physics and Chemistry.* **1963,** 67, 2030.

65. Thoresness , C.B.; Grens, E.A.; Sherwood, A. A one dimensional model for in situ coal gasification. *Lawrence Livermore Laboratory, University of California.* **1978**, 94550.

66. Skeel, R.D.; Bersins, M. A Method for the Spatial Discretization of Parabolic Equations in One Space Variable. *SIAM Journal on Scientific and Statistical Computing*. **1990**, 11, 1–32.